

Important Notice

This copy may be used only for the purposes of research and private study, and any use of the copy for a purpose other than research or private study may require the authorization of the copyright owner of the work in question. Responsibility regarding questions of copyright that may arise in the use of this copy is assumed by the recipient.

THE UNIVERSITY OF CALGARY

GROUP- AND PHASE-VELOCITY INVERSIONS
FOR THE
GENERAL ANISOTROPIC STIFFNESS TENSOR

by

Robert W. Vestrum

A THESIS
SUBMITTED TO THE FACULTY OF GRADUATE STUDIES
IN PARTIAL FULFILLMENT OF THE REQUIREMENTS FOR THE DEGREE OF
MASTER OF SCIENCE

DEPARTMENT OF GEOLOGY AND GEOPHYSICS

CALGARY, ALBERTA

MAY, 1994

© Robert W. Vestrum 1994

Abstract

Using forward models and geometrical analysis, criteria are established for deciding whether group or phase velocities are calculated from experimentally measured traveltimes in anisotropic samples.

With these results, two experiments were carried out: one to obtain phase velocities across an anisotropic sample; another to acquire group velocities across a second sample of the material. I designed numerical inversions for the 21 independent stiffnesses of the material from either group- or phase-velocity data. I then compared the accuracy, robustness and computational complexity of the two inversion procedures – group velocity to stiffnesses and phase velocity to stiffnesses.

My group-velocity inversion overcomes the difficulty of calculating group velocity in a prescribed direction and can calculate group velocities accurately even in directions near shear-wave singularities. Although phase velocities are easier to calculate than group velocities, the group-velocity inversion performed better in laboratory tests because group velocities are easier to measure.

Acknowledgements

First and foremost, I would like to thank my wife, Tammy, for her support and encouragement during my graduate work here at The University of Calgary. I am grateful for her helping me to maintain a balance between school and family life. I don't think I could have kept focussed without our four stress-relieving distractions, R.J., Aaron, Alex and Zoë.



I also must acknowledge the guidance and technical insights provided by Don Easley and the excellent technical support I received from Mark Lane and Darren Foltinek, two computer geniuses from the CREWES project. Eric Gallant, also with CREWES, was responsible for the manufacture of the anisotropic samples used in this study and was an invaluable resource when we were designing the experiments. I also wish to acknowledge the CREWES project and its sponsors for their financial support.

Thanks go also to my supervisor, Jim Brown, who gave me the encouragement and direction when I needed it and asked for it and otherwise gave me total freedom to pursue my own research projects and to do those projects using the methods and ideas of my choosing.

Doug Schmitt from the University of Alberta gave me the idea years ago to work on a complete inversion for all 21 of the elastic stiffnesses which define, in general, an anisotropic medium. I am grateful to him for introducing me to some of the concepts, ideas, and problems involved in seismic anisotropy.

I'd also like to thank Michael Musgrave for graciously offering a copy of his book, *Crystal Acoustics*, to me as a gift. This is an excellent book containing much of the foundations of seismic-anisotropy theory.

Table of Contents

Abstract	ii
Acknowledgements	iii
Table of Contents	iv
List of Tables	v
List of Figures	vi
Chapter 1: Introduction	1
1.1 Group and phase velocity in laboratory measurements	3
1.2 Relating velocities to stiffnesses	4
1.2.1 Velocities from stiffnesses	4
1.2.2 Symmetries	6
1.3 Inversion from velocities to stiffnesses	9
1.4 Laboratory investigations	11
1.5 Summary	11
Chapter 2: Group and Phase Velocities	13
2.1 The discrepancy in laboratory measurements	13
2.2 Numerical modelling method	16
2.3 Modelling results	17
2.3.1 Model plots	17
2.3.2 Geometry of the experiment	21
2.4 Conclusions from the numerical modelling study	24
Chapter 3: From Group or Phase Velocities to the General Anisotropic Stiffness Tensor	25
3.1 Method for calculating group velocities	25
3.2 Method for calculating stiffnesses	27
3.2.1 Stiffnesses from group velocities	27
3.2.2 Stiffnesses from phase velocities	29
3.2.3 Error analysis	30
3.3 Numerical testing of the algorithm	30
3.3.1 Phase-velocity inversion	31
3.3.2 Group-velocity inversion	32
3.4 Conclusions	34
Chapter 4: Application of the Inversion to Laboratory Measurements	35
4.1 Phase-velocity measurements	35
4.2 Group-velocity measurements	38
4.3 Why bother with two separate inversions?	41
4.4 Inversion for a not-so-general elastic tensor	42
4.5 Conclusions from the physical-model inversions	44
Chapter 5: Conclusions	47
References	51

List of Tables

2.1	Table of the angle between the group- and phase-velocity vectors (in degrees) for the three off-axis directions. The “% difference” figure is a measure of the difference between the magnitudes of the group and phase velocities. . . .	23
3.1	Stiffnesses used in calculating numerical velocity models for inversion testing.	31
3.2	Stiffnesses after 3 iterations of the phase-velocity inversion and final inverted stiffnesses with their respective error estimates.	32
3.3	Stiffnesses from the group-velocity inversion and their respective error estimates.	33
4.1	Stiffnesses estimated by phase-velocity inversion and their associated uncertainties.	37
4.2	Final inverted stiffnesses and their respective uncertainties from the group-velocity inversion of the laboratory data.	39
4.3	Stiffnesses from the group- and phase-velocity inversions of the same data. .	41
4.4	Differences between the group-velocity inverted stiffnesses and the phase-velocity inverted stiffnesses.	42
4.5	Final inverted stiffnesses and their respective uncertainties from the group-velocity inversion of the laboratory data assuming an orthorhombic medium. .	43

List of Figures

1.1	Definitions of group and phase velocities. The phase velocity, \mathbf{v} , is the velocity of the wave normal to the wavefront and the group velocity, \mathbf{g} , is the velocity of energy transport away from the source.	2
1.2	Orientation of symmetry planes for (a) cubic, (b) hexagonal, (c) orthorhombic and (d) monoclinic media. Modified from Crampin (1984).	7
2.1	Two wavefronts separated by unit time. The distances \mathbf{v} and \mathbf{g} travelled during that unit time represent the phase and group velocities, respectively.	14
2.2	Group and phase velocities of a wave propagating through the orthorhombic Phenolic CE.	14
2.3	The wavefront as represented by the group-velocity surface $\mathbf{g}(\phi)$ multiplied by the travelttime t . Note that the grey areas, the regions outside the plane-wave portion of the wavefront, are first arrivals from the edges of the transducer.	15
2.4	Three wave types propagating along the x axis: an axis of symmetry.	18
2.5	Wave propagation in the zx plane.	19
2.6	Wave propagation in the yz plane.	20
2.7	Wave propagation in the xy plane.	20
2.8	The geometric model for the phase-velocity measurement limit. (a) Group-velocity surfaces at progressive unit time steps (time units arbitrary). The curved portions of the wavefronts beyond the planar segments are shown in grey. (b) Geometry of this limiting case with the graphical definition of the maximum group-minus-phase angle δ_m	21
3.1	Plots of the velocity error from the phase-velocity inversion. (a) Velocity error versus number of iteration. (b) \log_{10} of the velocity error versus number of iteration.	31
3.2	Plots of the velocity error from the group-velocity inversion. (a) Velocity error versus number of iteration. (b) \log_{10} of the velocity error versus number of iteration.	33
4.1	(a) Bevelled cube of Phenolic CE. (b) The large transducers used to obtain phase traveltimes.	36
4.2	Phase-velocity plots for the phenolic block. The crosses represent the observed velocity data and the solid curves are the phase velocities computed from the inverted stiffnesses.	37

4.3	Experimental set-up for measuring group velocities on the sphere. In this jig, the sphere is clamped to a ring inside the protractor and can be rotated about a vertical axis at an increment measured on the protractors.	39
4.4	Group-velocity plots for the phenolic sphere. The crosses represent the data points from the experiment and the solid lines are the group velocities from the inverted stiffnesses.	40
4.5	Group-velocity plots for the phenolic sphere. The crosses represent the data points from the experiment and the solid lines are the group velocities from the orthorhombic stiffnesses.	44

Chapter 1

Introduction

Seismic anisotropy is the dependence of elastic-wave velocities through a medium on the direction in which the elastic wave is travelling. Conventionally, one might assume that elastic-wave velocities do not change with direction, i.e. that a particular medium is isotropic. However, this is not generally the case when, because of thin layering, fracturing, or crystal structure, there are some particular directions of travel in which the elastic-wave velocities will be faster or slower than in other directions of travel, i.e. that the material is anisotropic. When dealing with anisotropic materials, some very interesting and often nonintuitive effects are observed in the seismic waves and their velocities.

One of the effects of seismic anisotropy is the polarization and separation of transversely polarized or shear waves, a phenomenon called shear-wave splitting or birefringence. In wave propagation in isotropic elastic media, there are two types of body waves, longitudinal or compressional (P) and transverse or shear (S), characterized by the directions of oscillatory particle motion, or polarization, of the waves: longitudinal and transverse to the direction of wave propagation, respectively. The transverse particle motion of shear waves in isotropic media lies in a plane perpendicular to the direction of propagation and so, in general, may be resolved into two components. If these are in phase, the transverse motion is linear; if not the motion is elliptical.

In anisotropic media, the polarizations are not, in general longitudinal or transverse to the direction of wave propagation and, because of the differences of elastic properties with direction, the transverse wave will split into two quasi-shear (qS) waves with quasi-transverse polarizations which will, in general, propagate at different velocities. There are then, in general, three waves which propagate through an anisotropic medium called qP, qS₁, and qS₂, referring to the quasi-compressional or quasi-P wave and the fast and slow quasi-shear or quasi-S waves, respectively.

Another interesting effect of anisotropy is that the waves emanating from a point source are not, in general, spherical. Figure 1.1 shows part of a cross-section of a group-velocity surface for a qP wave propagating through a medium with cubic symmetry. The

group velocity, \mathbf{g} , is the velocity at which energy travels away from the source, so this curve also represents the shape of the wavefront of a wave travelling from a point source. If an observer were standing at the point A, the measured time on a stopwatch between the instant of the source disturbance and the instant the wave disturbance reached point A would be the group traveltime. The distance between the source and point A divided by the group traveltime will yield the group velocity. The group traveltime is defined simply as the traveltime that will yield a group velocity when divided into the distance between source and receiver.

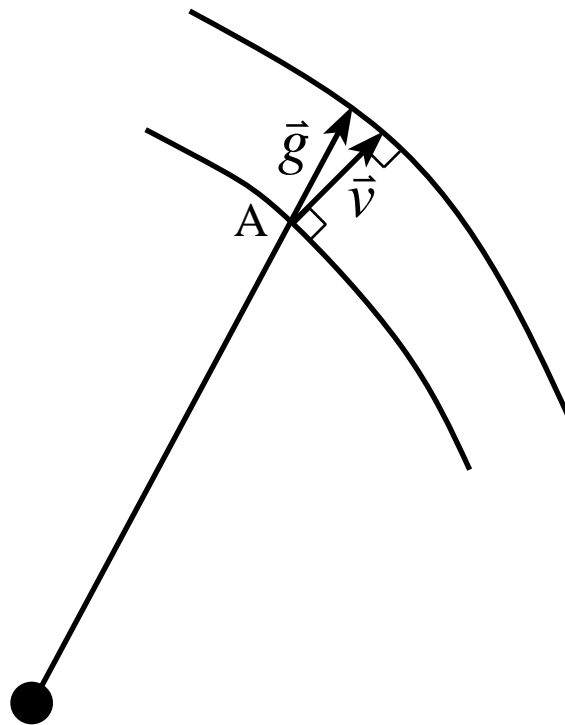


FIG. 1.1 Definitions of group and phase velocities. The phase velocity, \mathbf{v} , is the velocity of the wave normal to the wavefront and the group velocity, \mathbf{g} , is the velocity of energy transport away from the source.

If the observer standing at the point A did not know the timing or location of the source, and measured the velocity at which the wave propagated normally to a new position at a slightly later time, he would measure the phase velocity. The observer in this case measures a different velocity in a different direction than in the case where the group traveltime is measured with a stopwatch.

Because the phase velocity is the velocity normal to the wavefront, the easiest way a measured traveltime will yield a phase velocity is when the propagating waves are

plane waves and the measured traveltimes are divided into the distance the wave has travelled normal to the plane wavefront. The phase traveltime is then defined as a traveltime which, when divided into the distance travelled by the wave, yields the phase velocity.

1.1 Group and phase velocity in laboratory measurements

In the calculation of stiffnesses from measurements of traveltimes across anisotropic rock samples, it is important to know whether the distance across the sample divided by the traveltime yields a phase velocity or a group velocity. In anisotropic media, the group and phase velocities are, in general, not equal.

As discussed earlier, if we want to measure phase traveltimes, then we measure the traveltimes of plane waves across a sample and, if group traveltimes are desired, traveltimes from a point source to a point receiver should be measured. In laboratory measurements on anisotropic samples, finite-area transducers are used to transmit a signal across the rock sample; the infinitesimal point source and the infinite plane-wave source are not possible to create in the real world. If the transducers are large enough compared to their normal separation, they will transmit and receive plane waves over some large spatial interval and the traveltimes will yield phase velocities; if the transducers are very small compared to their separation, they will behave like a point source and a point receiver and their traveltimes will effectively yield group velocities.

The motivation for investigating the question of group and phase velocities in laboratory measurement comes from the previous physical-modelling studies done at The University of Calgary (Cheadle et al. 1991). The question of which of group or phase traveltimes were measured in the transmission experiments on the industrial laminate, Phenolic CE, was raised then. Cheadle et al. (1991) assumed that they were measuring group traveltimes since they measured the elapsed time for energy to travel from the source transducer to the receiver transducer. On further investigation prompted by Dellinger's (1992) work, I discovered that most of the measurements were phase traveltimes and a few of the traveltimes would not directly yield group or phase velocities.

The topic of group and phase velocities in laboratory measurements on Phenolic

CE and the criteria for deciding which are actually calculated from the traveltimes, based on the transducer sizes and separation, are discussed at length in chapter 2.

1.2 Relating velocities to stiffnesses

One of the goals of measuring the velocities of anisotropic materials is to determine their physical properties. Is the material strong or weak? If the material is hydrocarbon reservoir rock, is it fractured and is there a preferred orientation of the fractures? Questions like these can be answered if the elastic parameters, the stiffnesses, of the material can be calculated. First, the forward problem will be looked at: finding velocities from stiffnesses.

1.2.1 Velocities from stiffnesses

In order to arrive at a relationship between the elastic properties of a material and the seismic velocities through the medium (Shuvalov 1981; Beltzer 1988), the relation used is Hooke's law:

$$\sigma_{ij} = c_{ijkl}\epsilon_{kl} \quad 1.1$$

where σ and ϵ are the second-rank stress and strain tensors, respectively; c is the fourth-rank elasticity tensor; the elements of c are called the stiffnesses,¹ and there are, in general, 21 independent parameters that define the stiffnesses of the material. Einstein summation is implied.

Using $F = ma$ and the definition of strain, Hooke's law in terms of the displacement vector \mathbf{u} becomes the differential equation of motion:

$$\rho \ddot{u}_i = c_{ijkl} u_{l,jk} \quad 1.2$$

where ρ is the density of the material. Plane-wave solutions to this equation are of the form:

$$u_i = A_i f(\xi); \quad \xi = t - (\mathbf{n} \cdot \mathbf{r})/v = t - (n_j r_j)/v \quad 1.3$$

¹For reasons unknown to the author, c is commonly used for stiffness and s for compliance, the inverse of stiffness.

where v is the phase-velocity magnitude, \mathbf{n} is the wavefront normal or phase-velocity direction and \mathbf{A} is the polarization vector.

Upon substitution of the appropriate derivatives of the solution into the equation of motion, the resulting relation is Christoffel's equation which relates the phase velocity and particle motion or polarization to the density and elastic constants:

$$\rho v^2 A_i = c_{ijkl} n_j n_k A_l. \quad 1.4$$

A substitution is made in order to simplify the equation using the second-rank tensor:

$$\Gamma_{il} = c_{ijkl} n_j n_k \quad 1.5$$

to give the equation the form:

$$\Gamma_{il} A_l - \rho v^2 A_i = 0 \quad 1.6$$

which, due to the orthogonality of the polarization components, can be written in terms of the eigensystem:

$$(\Gamma_{il} - \rho v^2 \delta_{il}) A_l = 0. \quad 1.7$$

With a solution to this eigensystem (Press et al. 1988), the phase speeds, v , and the particle polarizations, \mathbf{A} , for the three wave phases, qP, qS₁ and qS₂, may be calculated for any given phase-velocity direction from the stiffnesses of the medium. From here, group velocities may be calculated from the stiffnesses of the material and the phase velocities. The equation for the group velocity was taken directly from Kendall and Thomson (1989) who give:

$$g_i = \frac{a_{ijkl} P_l D_{jk}}{D_{qq}}. \quad 1.8$$

The symbols in this compact notation are defined as follows:

$$a_{ijkl} = \frac{c_{ijkl}}{\rho}; \quad 1.9$$

$$p_l = \frac{n_l}{v}; \quad 1.10$$

and

$$D_{ij} = \frac{1}{6} \varepsilon_{ikl} \varepsilon_{jmn} \left(\frac{\Gamma_{km}}{\rho v^2} - \delta_{km} \right) \left(\frac{\Gamma_{ln}}{\rho v^2} - \delta_{ln} \right). \quad 1.11$$

Here c_{ijkl} is the stiffness tensor, ρ is the density, n_l is the l th component of the wavefront normal, v is the phase-velocity magnitude, and Γ_{ik} is defined in equation 1.6.

With these equations, group velocities and phase velocities may be calculated from any given set of stiffnesses. These forward-model velocities are used in a numerical inversion to estimate the stiffnesses of the material from the velocity measurements.

1.2.2 Symmetries

The stiffness tensor, c_{ijkl} , has $3^4 = 81$ elements which, because of the symmetries in the stiffness tensor and thermodynamic considerations (Nye 1957), reduce to 21 independent elastic stiffnesses. The stiffness tensor then is written (Voigt 1910; Nye 1957; Musgrave 1970; Thomsen 1986) as a second-order symmetric Voigt matrix:

$$c_{ijkl} \rightarrow C_{mn}$$

where

$$\begin{aligned} m &= i & \text{if } i &= j, \\ m &= 9 - (i + j) & \text{if } i &\neq j \end{aligned}$$

and

$$\begin{aligned} n &= k & \text{if } k &= l, \\ n &= 9 - (k + l) & \text{if } k &\neq l. \end{aligned} \quad 1.12$$

If there are spatial symmetries in the velocity variation of the material, these 21 independent parameters can be further reduced. In the case of spherical symmetry or isotropy, for example, the velocity is the same in all directions and there are only two independent elastic parameters. The other extreme is triclinic symmetry, where there is no symmetry in the velocities except the trivial symmetry which is a 180° symmetry about a point – the origin. This symmetry indicates that the velocity in one direction is identical to that in the exact opposite direction. The other symmetry cases that will be discussed here are cubic, hexagonal, orthorhombic, and monoclinic. The symmetry planes for media in these symmetry classes are shown in figure 1.2. For further discussion of the various symmetry classes, see Crampin (1984) or Winterstein (1990).

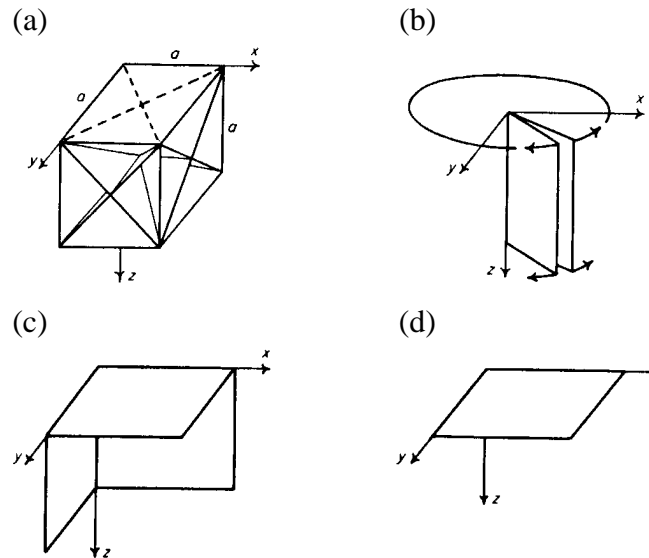


FIG. 1.2 Orientation of symmetry planes for (a) cubic, (b) hexagonal, (c) orthorhombic and (d) monoclinic media. Modified from Crampin (1984).

Crystals in the cubic symmetry class are optically isotropic, but elastically they are anisotropic (Helbig 1994). For media displaying cubic symmetry, there are three independent stiffnesses. The values of these three stiffnesses, a , b , and c , appear in the second-order stiffness matrix as shown:

$$C_{mn} = \begin{bmatrix} a & b & b & 0 & 0 & 0 \\ b & a & b & 0 & 0 & 0 \\ b & b & a & 0 & 0 & 0 \\ 0 & 0 & 0 & c & 0 & 0 \\ 0 & 0 & 0 & 0 & c & 0 \\ 0 & 0 & 0 & 0 & 0 & c \end{bmatrix}. \quad 1.13$$

In the case of hexagonal symmetry, also referred to in the elastic case as transverse isotropy, every plane containing the axis of symmetry is a plane of symmetry (see figure 1.2b). This implies that the velocities are identical in all horizontal directions. The five stiffnesses required to define a medium with this symmetry, a , b , c , d , and e , appear in the stiffness matrix in this manner:

$$C_{mn} = \begin{bmatrix} a & b & c & 0 & 0 & 0 \\ b & a & c & 0 & 0 & 0 \\ c & c & d & 0 & 0 & 0 \\ 0 & 0 & 0 & e & 0 & 0 \\ 0 & 0 & 0 & 0 & e & 0 \\ 0 & 0 & 0 & 0 & 0 & x \end{bmatrix}, \quad x = \frac{(a-b)}{2}. \quad 1.14$$

For orthorhombic symmetry, there are three mutually orthogonal planes of symmetry (see figure 1.2c). In this symmetry condition, there are nine independent elastic constants. This gives the following appearance to the second-order stiffness matrix:

$$C_{mn} = \begin{bmatrix} a & b & c & 0 & 0 & 0 \\ b & d & e & 0 & 0 & 0 \\ c & e & f & 0 & 0 & 0 \\ 0 & 0 & 0 & g & 0 & 0 \\ 0 & 0 & 0 & 0 & h & 0 \\ 0 & 0 & 0 & 0 & 0 & i \end{bmatrix}. \quad 1.15$$

A medium with monoclinic symmetry has only one symmetry plane (see figure 1.2d) and 13 elastic constants as follows:

$$C_{mn} = \begin{bmatrix} a & b & c & 0 & 0 & d \\ b & e & f & 0 & 0 & g \\ c & f & h & 0 & 0 & i \\ 0 & 0 & 0 & j & k & 0 \\ 0 & 0 & 0 & k & m & 0 \\ d & g & i & 0 & 0 & n \end{bmatrix}. \quad 1.16$$

One can see from equations 1.13 to 1.15 that cubic and hexagonal symmetries are special cases of orthorhombic symmetry where some of the coefficients of the matrix are equal or dependent on one or more of the other parameters.

An important thing to note here is that the stiffness matrices shown here have the orientation of the symmetry axes aligned with the coordinate axes. If we do not know in advance what the orientation of the symmetry axes are, all 21 elastic constants must be solved for and then coordinate-system rotations may be applied to the stiffness tensor to line the coordinate axes up with the axes of symmetry (Arts 1993). This process will yield the independent stiffnesses and the orientation of the symmetry planes or axes (if any).

1.3 Inversion from velocities to stiffnesses

The latest numerical inversion methods for calculating the 21 independent elastic stiffnesses from velocities have been proposed by Jech (1991), Arts et al. (1991) and Arts (1993). Jech's (1991) method is a least-squares inversion of qP-wave group velocities for stiffnesses and Arts' (1993) method involves a similar type of inversion using qP, qS₁ and qS₂ phase velocities to perform a generalized linear inversion (GLI) for stiffnesses. These two authors use similar linear-inversion techniques (the theory and method used in the inversion for this thesis are discussed in chapter 3). Other stiffness-determination procedures have been proposed by Neighbours and Schacher (1967) and Hayes (1969).

Arts (1993) performs his inversion for the stiffnesses of what is referred to as a general anisotropic medium, meaning a medium where nothing is assumed about the 21 independent elastic stiffnesses. He identifies the major problem with inverting from group velocities in his discussion as to why he chose to invert from phase velocities. The group velocities, in general, cannot be calculated directly in a prescribed direction, so an iterative procedure must be used to find the group velocity in a particular direction.

In Arts' inversion, which is very similar to the inversion by van Buskirk et al. (1986), he solves Christoffel's equation (equation 1.4) for the stiffnesses in terms of the phase velocities, the wavefront normals and the polarizations. He acknowledges, however, that it is very difficult, if not impossible, to obtain accurate measurements of polarizations. An iterative procedure is then performed to improve the estimate of the polarization vectors by minimizing the difference between the phase velocities calculated from the inverted stiffnesses and the observed phase velocities. This iterative procedure is

the improvement added by Arts et al. (1991) to the van Buskirk et al. (1986) inversion, which requires an accurate particle-displacement measurement.

Because his inversion requires phase-velocity observations, Arts (1993) makes traveltime measurements between large opposing faces of a truncated cube with the assumption that he can generate plane waves across the sample between the faces. This limits his measurement of traveltimes to certain directions where faces have been cut into the sample. The upper limit on the number of observations for the inversion imposed by his experiment is 27, nine measurements of each of the three wave phases (qP, qS₁, qS₂).

Jech (1991) has overcome the difficulty involved in calculating the group velocity in a prescribed direction by using an iterative method to find the group velocity given a particular direction. He uses only qP-wave velocities in his inversion technique, likely because of the difficulty in finding qS-wave velocities. Jech (1991) says “a problem arises for quasi-shear [qS] waves, as there is a danger that we may not follow the right value of the normal [phase] velocity of two quasi-shear waves in regions where the normal velocity surfaces of two quasi-shear waves intersect.” He goes on to propose that if one kept track of the particle polarizations during a search for a group velocity, one could discriminate between the two qS waves. This would not, in general, work because when two qS phase-velocity surfaces intersect, the polarizations usually change dramatically in any type of anisotropic medium.

Jech’s inversion method is a straightforward GLI which is somewhat similar to the method outlined in chapter 3 of this thesis. The main difference between the methods is the use of the qS₁ and qS₂ velocities.

In the method proposed in this thesis, a standard least-squares inversion is employed to find the stiffnesses which yield the best fit to the observed velocities. The same method is used for the group-velocity inversion as for the phase-velocity inversion, but there is an additional step involved in finding the group velocity in a prescribed direction when performing the group-velocity inversion.

No regard is given to the polarization vectors in the inversion developed in this thesis; they can’t effectively be measured and they behave unpredictably at times, so they are not considered in these inversion procedures. The criterion for establishing which velocity belongs to which phase is the order of highest to lowest velocity or from first to last arriving wave phase. The first arriving phase is qP, next is qS₁ and last arriving wave phase with the slowest velocity is defined as qS₂.

1.4 Laboratory investigations

The laboratory experiments were performed to test the inversion algorithm. Material used in this physical modelling is Phenolic CE, an industrial laminate. This material consists of canvas layers which are saturated and bonded together by phenolic resin. The layers are woven in such a way that the canvas fibers are straight in one direction whereas the fibers in the direction orthogonal to the straight fibers weave or curl over and under the straight fibers. There has already been work done on this material (Brown et al. 1991, 1993; Cheadle et al. 1991) where the material is assumed to have orthorhombic symmetry.

The symmetry planes are assumed to be oriented with one in the plane of the layers and two orthogonal to this plane, one parallel to the curly fibers and one parallel to the straight fibers. The Cartesian coordinate system used here for this material has the z axis normal to the canvas layers, the y axis in the direction of the straight fibers and the x axis in the direction of the curly fibers. The x axis is the direction of maximum qP-wave velocity, the y axis that of intermediate qP-wave velocity and the z axis that of slowest qP-wave velocity. This is due to the layering and the woven nature of the fabric. When convenient, spherical coordinates are used with Θ being the angle of colatitude measured from the z axis and Φ is the angle of azimuth from the x axis.

Since the inversion developed here is general, i.e., assuming no symmetry, the assumption of orthorhombic symmetry can be investigated. In this investigation, an inversion for the nine independent orthorhombic stiffnesses is performed and the results are compared to the general inversion to determine whether or not the inversion incorporating the assumption of orthorhombic symmetry produces a solution as good as the inversion for the general anisotropic stiffness tensor.

1.5 Summary

In anisotropic media, group and phase velocities are not, in general, equal. This difference raises the question of which of group or phase traveltimes are measured in laboratory experiments. The simple assumption that the time taken for energy to propagate from a finite source to a finite receiver must be a group traveltime has been

shown to be invalid (Dellinger 1992). It is important to know just what traveltimes one is measuring because the difference between group and phase velocities makes a substantial difference in the process of inverting velocities for stiffnesses of a material.

In chapter 2 the question of group versus phase velocities in lab measurements is discussed. Using numerical models and the geometry of the experiments done by Cheadle et al. (1991), a criterion is established to determine which of group or phase traveltimes are measured.

In order to compare the applicability of the two measurements – of group traveltimes and of phase traveltimes – to determining stiffnesses, numerical inversion processes were developed which calculate stiffnesses from either group or phase velocities. The development and testing of these inversions are outlined in chapter 3.

Armed with the information about how to measure group and phase traveltimes from chapter 2 and the inversion routines from chapter 3, laboratory experiments were designed to acquire group and phase traveltimes through the Phenolic CE and the inversion programs were tested on laboratory data. Chapter 4 gives the results of these inversions and a discussion on the assumption that the phenolic material displays orthorhombic symmetry.

Chapter 2

Group and Phase Velocities

Physical modelling experiments have been performed by Cheadle et al. (1991) on the Phenolic CE which was assumed to have orthorhombic symmetry. In such experiments, transit times across a sample are measured with the goal of calculating velocities in the material which are then used to calculate the stiffnesses of the material. The question arises, however, as to whether the velocities determined in the normal way, i.e. by dividing distance between the transducer faces by traveltime, are group velocities, phase velocities, or some combination thereof.

Any dynamic effects investigated in this study of the source and receiver finiteness are only in the transit times. The only important observations that are made are the elapsed time between the excitation of the source and the first pulse arrival at the receiver and the distance between source and receiver.

2.1 The discrepancy in laboratory measurements

The question of group versus phase velocities arises from the wave effects due to the source and receiver transducer sizes (Dellinger 1992). In the case of a plane seismic wave propagating through a solid, the traveltime measured across the sample in the direction normal to the wavefront will be the phase velocity. With a wave propagating from a point source, the group or energy velocity will be measured in any direction away from that source using a point receiver. With the finite transducer source and receiver that is used in physical modelling work, there will be some portion of the wavefront that is flat like a plane wave (Musgrave 1959) and the rest of the wave surface will be in the shape of the group-velocity surface.

The orthorhombic medium has, by definition, three mutually perpendicular axes of symmetry. There is symmetry under any rotation of 180° about a symmetry axis, i.e. two-fold symmetry. In these symmetry directions, which were chosen for three of the six measurement directions, the group and phase velocities are equal.

Figure 2.1 shows an example of the difference between group and phase velocity

in terms of the propagation of the wavefront in an anisotropic medium. The diagram shows two wavefronts in space that are separated by unit time. The distance that the wavefront has travelled in unit time along a particular ray emanating from the source is labelled \mathbf{g} , for group velocity. The normal distance between the two wavefronts is labelled \mathbf{v} , for phase velocity.

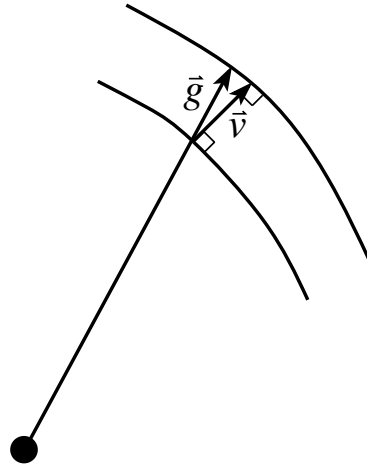


FIG. 2.1 Two wavefronts separated by unit time. The distances \mathbf{v} and \mathbf{g} travelled during that unit time represent the phase and group velocities, respectively.

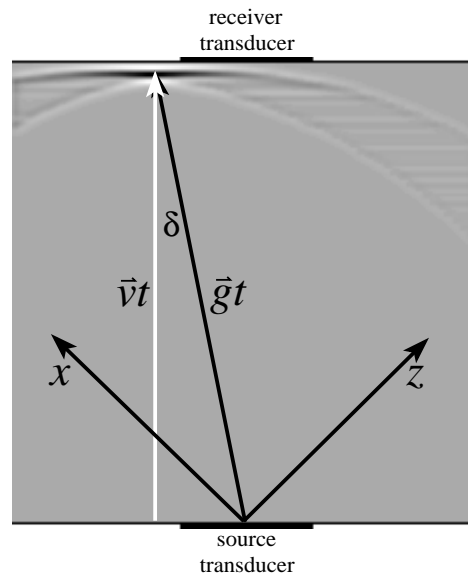


FIG. 2.2 Group and phase velocities of a wave propagating through the orthorhombic Phenolic CE. The white vector, labelled $\mathbf{v}t$, represents normal distance travelled by the wave moving at the phase or normal velocity in time t whereas \mathbf{g} is the corresponding group or energy velocity and $\mathbf{g}t$ is the corresponding distance of energy transport from the source in the same time t .

Figure 2.2 shows a plot of the wave propagating away from a relatively large source transducer. The group-velocity vector, labelled here as \mathbf{g} , represents the velocity of energy transport outward from the source. The vector \mathbf{v} in white is the phase or normal velocity vector and shows the velocity of the plane wave across the sample in the direction normal to the wavefront. In this example the source and receiver diameters are 4 cm and the distance between the centres of their faces is 14 cm. This sideslip effect has been demonstrated in laboratory experiments by Markam (1957).

It can be seen for this sample (figure 2.2) that the transit time recorded and the normal separation measured will yield phase velocity across the sample. That is, the first pulse arriving at the receiver will be from the plane-wave portion of the wavefront. If the receiver transducer had been located a bit to the left so that the line joining the centres of the source and receiver transducers were in the direction of \mathbf{g} , the transit time would represent the group velocity.

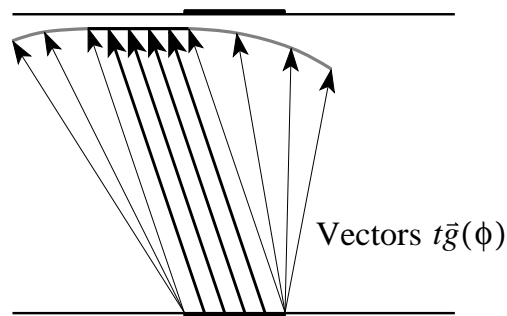


FIG. 2.3 The wavefront as represented by the group-velocity surface $\mathbf{g}(\phi)$ multiplied by the traveltime t . Note that the grey areas, the regions outside the plane-wave portion of the wavefront, are first arrivals from the edges of the transducer.

Figure 2.3 shows a schematic of a wavefront as the group-velocity surface multiplied by the traveltime t . The grey areas of the wavefront in this figure represent the leading edge of the low-amplitude region of figure 2.2. The grey regions come from the edges of the transducer, as seen in the distribution of group-velocity vectors in figure 2.3. The bolder vectors that show the travel of the plane-wave portion of the wavefront are parallel and there is a high concentration of energy in this plane-wave portion since there is no geometrical spreading in the propagation of a plane wave. One can see from this geometry that if the traveltime is measured by observing the arrival of the grey area of this wavefront, the raypath used when calculating the group velocity cannot be assumed to be a line between the centres of the transducers.

2.2 Numerical modelling method

In a numerical investigation of the measurements made on the phenolic block, the wavefield is calculated in the same way as in figure 2.2 in order to determine what sort of velocity is obtained from the division of transducer separation by traveltime. When calculating the position of the wavefront emanating from the transducer, the transducer is divided up into small discrete elements; a wavefront is calculated for each element and these are then summed over the source transducer.

In acquiring the wavefront for each element, the group- or ray-velocity surface is calculated. The wavefront is then assumed as the group-velocity surface scaled by the traveltime. Using the ray-velocity surface as the wavefront is called the ray approximation and is valid as a far-field approximation in homogeneous media. In order to derive the group-velocity surface, Christoffel's equation is solved for the phase velocity. This equation is an eigensystem of the form

$$\Gamma \mathbf{A} = \rho v^2 \mathbf{A}. \quad 2.1$$

The tensor Γ is real and symmetric, thereby giving real and positive eigenvalues which are equal to the density times the square of the phase velocity (ρv^2), and the eigenvectors are the respective polarization vectors \mathbf{A} . Γ is defined as a function of the elastic constants (stiffnesses) of the material, c_{ijkl} , and the unit wavefront-normal vector \mathbf{n} , as follows:

$$\Gamma_{ik} = c_{ijkl} n_j n_l; \quad 2.2$$

$$i, j, k, l = 1, 2, 3.$$

Once the phase-velocity surface is known, where v is the magnitude and \mathbf{n} defines the direction of the phase-velocity vector, the group-velocity surface can be derived. Since the traveltime measurements for the purpose of deriving the elastic constants are performed in assumed symmetry planes, the angle between group and phase velocity is confined to that plane. The two-dimensional relationship between the group velocity, \mathbf{g} , and phase velocity, \mathbf{v} , in symmetry planes is given by many authors (e.g. Postma 1955; Brown et al., 1991; Dellinger 1991) as

$$g = \sqrt{v^2 + \left(\frac{\partial v}{\partial \theta}\right)^2}, \quad 2.3$$

where θ is the angle of the phase vector \mathbf{v} in a symmetry plane. The group angle ϕ in this plane is given by:

$$\phi = \theta + \arctan\left[\frac{(\partial v/\partial \theta)}{v}\right]. \quad 2.4$$

In the computer program written for this study, the group-velocity surface is calculated once and then that surface is added into the data grid for each element of the source. Geometrical spreading of the amplitude is approximated by the inverse of the distance travelled along a given raypath. The resulting wavefront is convolved with a Ricker wavelet with a dominant frequency of approximately 600 kHz, which is the dominant frequency of the transducers used in the laboratory experiments on the orthorhombic medium. The transducers were sized at 12.6 mm in diameter, the phenolic cube was assumed 10 cm across each side and 11.55 cm across the diagonal directions between bevelled edges. The elastic constants, density of the material, geometry of the experiment and the frequency of the ultrasonic waves were all taken from the Cheadle et al. (1991) paper.

The resulting plots are of a wavefront in the plane of symmetry that has travelled roughly 98% of the distance from source to receiver in the quasi-compressional (qP) and quasi-shear (qS₁ and qS₂) cases. The same elapsed time was used for qS₁ and qS₂. From here it can be interpreted whether or not the travelttime recorded between source and receiver represents the group or the phase velocity across the sample. The program also calculates the angle between the group velocity and the direct path between source and receiver that is normal to both transducer faces in these experiments.

2.3 Modelling results

2.3.1 Model plots

Plots have been generated for qP, qS₁ and qS₂ waves for six propagation directions in the sample, that is, along each symmetry axis and along the three diagonal

directions in symmetry planes at 45° from the symmetry axes. For example, the measurement direction between the x and y axes at 45° to each axis is referred to as the xy direction. In this study, the x , y , z , yz , zx , and xy directions correspond to the 1, 2, 3, 4, 5 and 6 directions of Cheadle et al. (1991).

Figure 2.4 shows a triad of plots for the more straightforward case, which is the measurement along a symmetry axis. These plots are cross-sections in the zx plane with the x axis running vertically between source and receiver. In these plots, where the measurement of seismic wave propagation is along a symmetry axis, the group and phase velocities are equivalent, as mentioned earlier. The question of whether group or phase velocity – or neither – is being determined arises when the experiment is carried out in the off-symmetry directions.

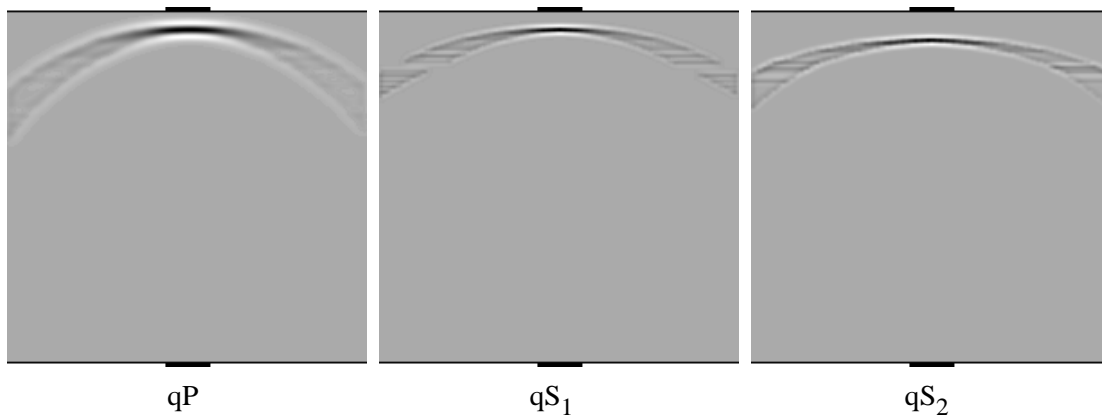


FIG. 2.4 Three wave types propagating along the x axis: an axis of symmetry.

An interesting example of the off-symmetry measurement is the wave propagation in the zx plane. The x and z axes are the directions of highest and lowest qP-wave velocity so this symmetry plane displays the greatest qP-wave anisotropy. Figure 2.5 shows the wavefront plot triad for the measurement in the zx direction.

It can be seen here (figure 2.5) that the group and phase velocities are not equivalent in this measurement direction. The flat plane-wave portion of the wavefront for the qP wave is moving to the left, just as was seen in figure 2.2. The difference between this wavefront and that in figure 2.2 is caused by the difference in the size of the transducers. Here (figure 2.5) the transducers are 12.6 mm in diameter which is significantly smaller than the 40-mm diameter transducers that are used in figure 2.2. Using this smaller transducer, it appears that the plane-wave portion of the wavefront

does not hit the receiver transducer. One can conclude from figure 2.5 that, to determine the qP-wave group velocity, the correct distance of travel to be used is the distance from the right edge of the source to the left edge of the receiver.

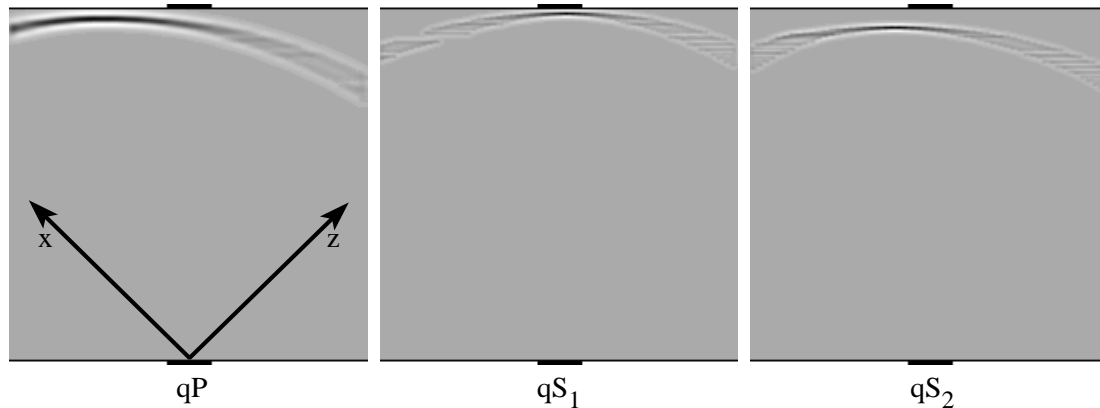


FIG. 2.5 Wave propagation in the zx plane. Coordinate axes are shown in the qP-wave plot.

In the qS-wave cases, there is less anisotropy observed than in the qP-wave cases and it appears that the phase velocity will be measured for these polarizations in this measurement direction. The plane-wave portion of the wavefront will be observed as the first impulse at the receiver transducer and therefore the distance across the sample divided by the observed traveltime will yield the correct phase velocity.

For the yz plane (figure 2.6), the observable anisotropy is a little smaller than appears in the zx plane. The z direction is normal to the layers of fabric and is the direction with the lowest qP velocity, 2925 m/s, substantially lower than the qP velocity in either the x or y direction, 3576 m/s and 3365 m/s respectively. The degree of P-wave anisotropy in the yz plane is 15%, which is less than the 22% P-wave anisotropy in the zx plane.

Figure 2.6 shows that there will be a phase velocity measured for both qS₁ and qS₂ and possibly a group velocity for the qP wave in the yz plane. However, there is some question as to which of group or phase velocity will be measured for the qP. The edge of the plane-wave portion may be observed at the receiver. Is there a region on the wavefront for which neither group nor phase velocity is measured? The answer to this would be yes if we always used the distance between centres of transducer faces in calculating velocity, without thinking any further, but this is not necessary. Group velocity can always be calculated from the measured traveltime, even with finite transducers: there is, however, an uncertainty in the length of the raypath which has to be

resolved. This will be further discussed below using geometrical arguments.

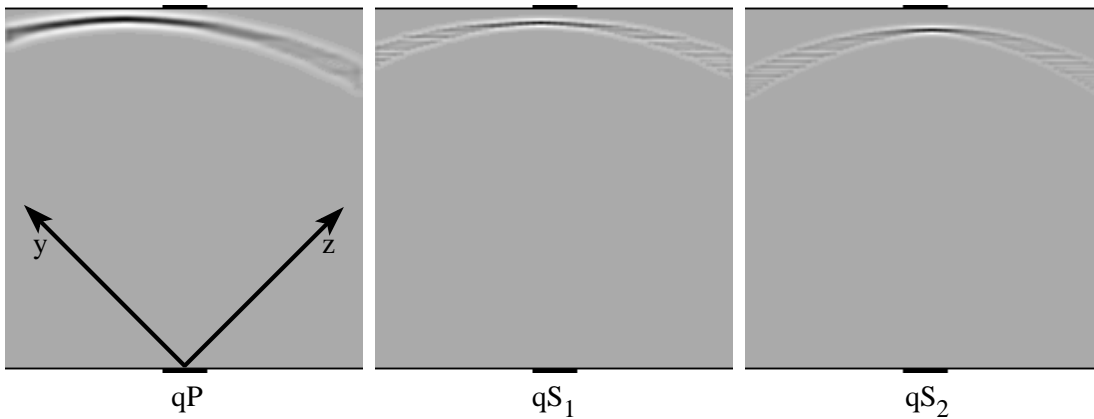


FIG. 2.6 Wave propagation in the yz plane. The coordinate axes are shown in the qP -wave plot.

What can be concluded from these plots is that the quasi-shear-wave measurements will directly yield a phase velocity and the qP -wave measurement will likely give a group velocity.

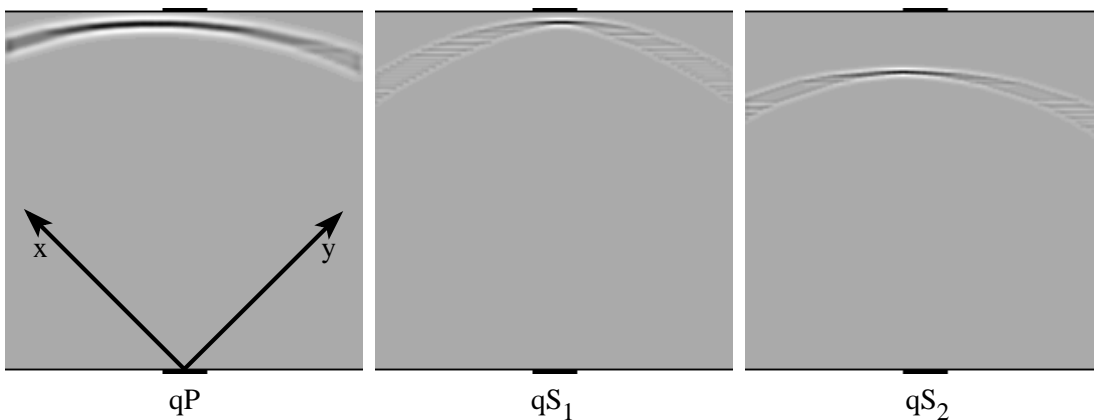


FIG. 2.7 Wave propagation in the xy plane. The coordinate axes are shown in the qP -wave plot.

The last diagonal measurement is in the xy plane where the velocity anisotropy is caused by the nature of the woven fabric. The least qP -wave anisotropy is observed in this plane where the difference between qP -wave velocities is only 6%. From the plots of the wavefronts propagating in this symmetry plane (figure 2.7), it can be assumed that the measured traveltime across the sample represents the phase velocity. In each case, there will be an arrival of the plane-wave portion of the wavefront at some part of the receiver.

Note that in this plane, the shear-wave splitting is relatively large as shown by the difference in the distance travelled by the two wave types. In this case, the qS_2 is polarized in a direction near the vertical, or close to the z direction which is the slowest qP -wave direction in this sample.

From the plots of the wavefronts in the sample of Phenolic CE, it has been observed that in most cases the phase velocity has been measured. The exceptions occur when there is a large velocity anisotropy, as with the qP -wave measurement in the zx and yz directions. In this case the traveltime measurement may be indicative of a group velocity. If a medium displayed more pronounced anisotropy than what has been observed here, then one could be confident that these measurements would, indeed, yield group velocity.

2.3.2 Geometry of the experiment

One other form of output from this analysis is the angle between the group- and phase-velocity vectors. This is also the angle between the group-velocity vector and the normal to the transducer faces. This angle will indicate where the edge of the plane-wave portion of the wavefront is.

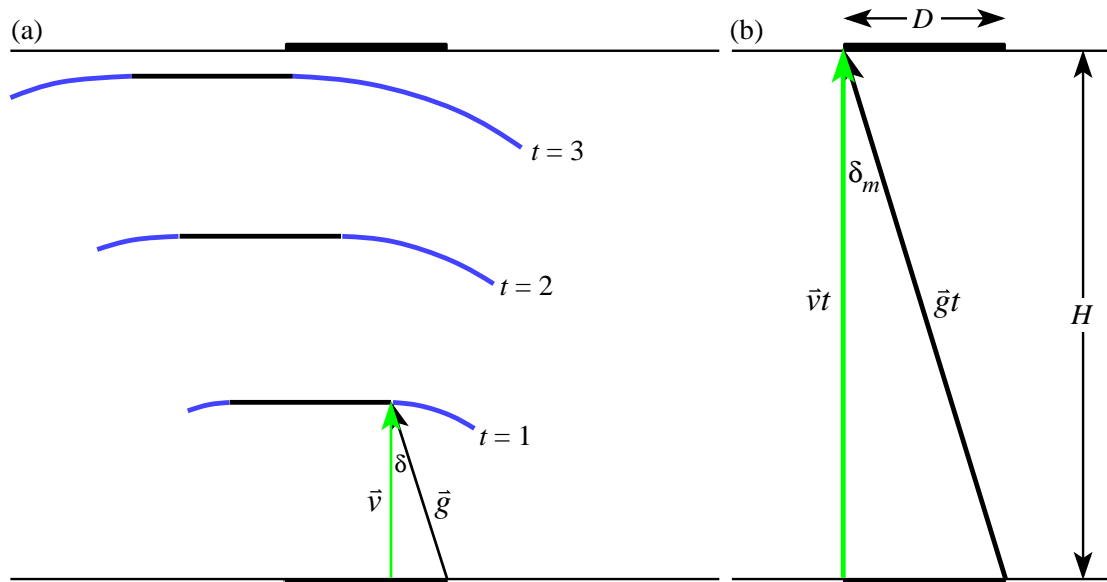


FIG. 2.8 The geometric model for the phase-velocity measurement limit. (a) Group-velocity surfaces at progressive unit time steps (time units arbitrary). The curved portions of the wavefronts beyond the planar segments are shown in grey. (b) Geometry of this limiting case with the graphical definition of the maximum group-minus-phase angle δ_m .

Consider a seismic wave propagating from a source transducer in a symmetry plane in a direction such that the angle between the group- and phase-velocity vectors,

$$\delta = \phi - \theta, \quad 2.5$$

is equal to δ_m . Figure 2.8a shows a wavefront propagating from the transducer at the bottom of the figure and the associated plane phases. The plane phases and the plane-wave portion of the wavefront are in black. Figure 2.8b defines the angle δ_m as the maximum angle between the group and phase velocities where there will be some plane-wave observed at the receiver. From the geometry of the figure, this maximum angle is given by:

$$\delta_m = \arctan\left(\frac{\text{transducer diameter}}{\text{height of sample}}\right). \quad 2.6$$

It is apparent from this illustration that, when δ is greater than δ_m , none of the planar wavefront portion will be observed at the receiver. Rather, the receiver in this case will be illuminated only by the curved grey area of the wavefront (figure 2.8a) which is a group-velocity surface. This grey portion of the wavefront to the right of the black plane-wave portion comes from the right-hand edge of the source transducer which, when considering the first arrival of energy, behaves like a point source. A group velocity is clearly measured in this case. The raypath is not vt (figure 2.8b), the distance between the faces of the transducers, but is gt , the oblique raypath from the right edge of the source transducer to the left edge of the receiver transducer.

Once the angle δ becomes greater than δ_m , the measured traveltime is no longer indicative of the phase velocity. In this case, the velocity, if determined by dividing the normal transducer separation by the traveltime, will be something between phase and group velocity, as indicated by Dellinger (1992). But if one is able to determine the actual distance travelled in the oblique ray or group direction, one will be able to calculate the group velocity. The maximum such distance, corresponding to $\delta = \delta_m$, will be

$$\sqrt{D^2 + H^2}.$$

Therefore, the maximum difference, ε , between this and the normal separation will be

$$\varepsilon = \sqrt{D^2 + H^2} - H. \quad 2.7$$

One can see from this equation that for large samples and small transducers, this pathlength difference goes to zero and, in effect, a group traveltime will always be measured without worry of transducer effects. The maximum error in the raypath length for the experimental geometry used in this study, $\varepsilon = 0.7$ mm, is fairly small compared to the size of the 115.5 mm sample.

Table 2.1 shows the angle δ , group-minus-phase angle, for each measurement in the experiment. Additional data in this table are the percentage differences between the group and phase velocities. This table shows that there is very little difference in the magnitudes of the group and phase velocities in the off-symmetry directions of this medium; there is a maximum near 2% for the qP wave in the zx direction.

Using equation 2.6, δ_m is calculated as 6.22° for $H = 115.5$ mm and $D = 12.6$ mm. The only waves for which $\delta > \delta_m$ are the qP waves measured in the zx and yz directions. From the analysis of the plots, it was determined that all but these two wave measurements would be measuring phase velocity. This geometrical analysis is fast and simple and appears to agree with the conclusions made from the interpretation of the wavefront plots.

		xy direction		zx direction		yz direction	
		angle	%difference	angle	%difference	angle	%difference
Wave Type	qP	4.11	0.257%	11.63	2.053%	8.49	1.096%
	qS1	0.63	0.006%	0.57	0.005%	0.98	0.015%
	qS2	1.65	0.041%	2.62	0.105%	0.68	0.007%

TABLE 2.1 Table of the angle between the group- and phase-velocity vectors (in degrees) for the three off-axis directions. The “% difference” figure is a measure of the difference between the magnitudes of the group and phase velocities.

Cheadle et al. (1991, p 1608) calculated the phase angle, θ , from which the angle δ may be calculated. With this information and equation 2.6, which gives δ_m as a function of the experimental geometry, this geometrical analysis could have been applied to determine whether group or phase velocities were measured by comparing calculated δ values with δ_m .

An important conclusion may be drawn from this geometrical analysis of the propagation of the wavefront. For elastic-property determination, it is desirable to measure phase velocity between the source and receiver. If large source and receiver transducers are used, then the experimentalist can be confident that it is, indeed, a traveltime that will yield the phase velocity in the normal direction between transducer faces. With relatively small finite-area source and receiver transducers, there will always be some uncertainty, not only in the distance that the wave has travelled at the group velocity, but also in the calculated group-velocity direction. In measuring properties of anisotropic materials where the seismic velocities change with direction, this directional error may be significant.

2.4 Conclusions from the numerical modelling study

From the interpretation of wavefront plots based on a ray model and from geometrical arguments it has been shown that, for most cases in the off-symmetry directions, Cheadle et al. (1991) have measured phase velocity in the orthorhombic medium. The effects caused by assuming group velocity were seen to be relatively small in that the difference between group and phase velocity of this medium is 2% or less.

A geometrical argument defined a maximum angle between group and phase velocity vectors for which the phase traveltime can be observed. In this case, the geometrical analysis yielded the same results with regard to the question of group or phase velocities as did the modelling study. This geometric method is a fast and easy way to determine which velocity type may be directly calculated from the traveltimes.

Chapter 3

From Group or Phase Velocities to the General Anisotropic Stiffness Tensor

The numerical scheme for inverting for the stiffness tensor used here is general in the sense that there is no assumption made of the symmetry class of the medium or the orientation of the symmetry axes. From group-velocity traveltimes measurements of qP , qS_1 and qS_2 waves the stiffnesses for the medium are estimated using a generalized linear inversion (GLI).

The difference between this numerical scheme and others recently proposed (Jech 1991; Arts 1993) is that the stiffnesses are calculated based on the traveltimes and are independent of the particle polarization directions, which can be difficult to measure and which can vary rapidly in even mildly anisotropic media. Also, like Jech's (1991) method, this method has the additional complication of using the group velocities in the inversion.

As shown in chapter 2, some laboratory measurements yield group velocities and others yield phase velocities. The velocities calculated from VSP surveys are also group velocities. This inversion from either group or phase velocities is specifically designed for the inversion of laboratory-measured group traveltimes and may be useful in the case of the multicomponent VSP survey where there are ray-velocity measurements at a broad range of angles through, for example, a fractured reservoir.

3.1 Method for calculating group velocities

With a given set of stiffnesses the magnitude of the group or ray velocity cannot be explicitly calculated in a particular direction. On the other hand, given the stiffnesses and a wave normal, the phase velocity may be calculated analytically. With this phase-velocity information, the group velocity associated with that particular phase velocity may be calculated. The group velocity does not, in general, lie in the same direction as

the wave normal or the phase-velocity direction, as shown in chapters 1 and 2. The group velocity is dependent on the phase-velocity magnitude, v , and the phase-velocity direction or wavefront normal vector, \mathbf{n} , from equations 1.8 and 1.10. If the group velocity is to be calculated in a prescribed direction, a search must be performed to find a phase-velocity vector which will yield a group velocity in the desired direction.

This is the first task performed by the least-squares inversion method. In the search for a group velocity in the prescribed direction, a guess is made for the phase-velocity direction, in the spherical coordinates Θ (colatitude relative to the z axis) and Φ (azimuth relative to the x axis) associated with the desired group-velocity direction. In the first-order approximation, the observed group-velocity vector, \mathbf{g}^{obs} , and the calculated group-velocity vector, \mathbf{g}^{calc} , from the guessed Θ and Φ are related by:

$$g_i^{obs} = g_i^{calc} + \frac{\partial g_i}{\partial \Theta} \Delta\Theta + \frac{\partial g_i}{\partial \Phi} \Delta\Phi. \quad 3.1$$

In this equation, the only unknowns are $\Delta\Theta$ and $\Delta\Phi$, the errors in the Θ and Φ estimates. The partial derivatives are calculated numerically.

If matrix notation is used, such that

$$\tilde{\delta}\mathbf{g} = \begin{bmatrix} g_x^{obs} - g_x^{calc} \\ g_y^{obs} - g_y^{calc} \\ g_z^{obs} - g_z^{calc} \end{bmatrix}, \quad \tilde{\alpha} = \begin{bmatrix} \frac{\partial g_x}{\partial \Theta} & \frac{\partial g_x}{\partial \Phi} \\ \frac{\partial g_y}{\partial \Theta} & \frac{\partial g_y}{\partial \Phi} \\ \frac{\partial g_z}{\partial \Theta} & \frac{\partial g_z}{\partial \Phi} \end{bmatrix}, \quad \text{and } \tilde{\Delta} = \begin{bmatrix} \Delta\Theta \\ \Delta\Phi \end{bmatrix}, \quad 3.2$$

then we get an equation in the form:

$$\tilde{\delta}\mathbf{g} = \tilde{\alpha} \tilde{\Delta} \quad 3.3$$

which has a solution in the standard least-squares form (Twomey, 1977) given by

$$\tilde{\Delta} = [\tilde{\alpha}^T \tilde{\alpha}]^{-1} \tilde{\alpha}^T \tilde{\delta}\mathbf{g}. \quad 3.4$$

Once values for $\Delta\Theta$ and $\Delta\Phi$ are estimated using this technique, they are then added to the initial guesses and the process is repeated. The iterations continue until a

group velocity is calculated in a direction within some allowable deviation from the desired direction or the changes in the angles Θ and Φ decrease to within an acceptable tolerance level.

In performing this least-squares inversion, group velocities, \mathbf{g}^{calc} , are calculated using Kendall and Thomson's (1989) equation (equation 1.9) and the stiffnesses and density of the material.

Because of the unpredictable behaviour of the polarizations of the different wave phases, the decision as to which wave phase is associated with a particular velocity is made using the which-came-first criterion. The wave with the highest velocity is assumed to be the qP, the second fastest phase is considered the qS₁ and the slowest wave phase will then be the qS₂.

The only problem with this method is in the difficulty in finding a solution close to a shear-wave singularity. At a point singularity or conical point (see Brown et al. 1993), the first derivative of the velocity with respect to Φ or Θ is discontinuous, which can make searching around these point singularities unstable. Near singularities or other problem areas on the wave surface where this search method fails, the program switches into a recursive random search in an attempt to find the appropriate group velocity.

Computationally intensive and limited in accuracy, this method pays no attention to the shape of the surface and can get the search algorithm within a degree or two from the desired group direction. The routine calculates 500 points chosen in a Gaussian distribution around an initial-guess direction. The point with a group-velocity direction closest to the desired direction is taken as the new mean and the standard deviation of the Gaussian-distributed random search is decreased by a factor of five and the search starts over. This process continues until a solution is found or there is little improvement.

In most cases, the GLI method will converge if the random search can get close enough to the desired group direction. Occasionally the GLI will still diverge and the program has to settle for a group velocity that is usually in a direction less than 1° from the desired direction.

3.2 Method for calculating stiffnesses

3.2.1 Stiffnesses from group velocities

The previous application of this linear-inversion technique was merely to calculate a group-velocity vector in a prescribed direction. In the inversion for the

stiffnesses, the approach taken is similar to the method used in calculating the group velocity.

It is similar because the problem is essentially the same. The goal is to minimize the difference between the observed group velocities and the calculated group velocities. The relationship between the i th observed group-velocity magnitude and the i th calculated group-velocity magnitude is:

$$g_i^{obs} = g_i^{calc} + \frac{\partial g_i}{\partial C_j} \Delta C_j \quad 3.5$$

where C_j is the j th independent stiffness, $j = 1, 21$. Using the matrix notation:

$$\delta g_i = g_i^{obs} - g_i^{calc}, \quad \alpha_{ji} = \frac{\partial g_i}{\partial C_j}, \quad \text{and } \Delta_i = \Delta C_i, \quad 3.6$$

the difference between the observed and calculated group velocities can be expressed in an equation of the same form as equation 3.4:

$$\bar{\Delta} = [\bar{\alpha}^T \bar{\alpha}]^{-1} \bar{\alpha}^T \bar{\delta}g.$$

This is a similar mathematical problem as in section 3.1, except that now the g_i^{calc} and g_i^{obs} are the i th magnitudes of the calculated and observed group velocities, respectively, instead of the i th components of a group-velocity vector as defined in equation 3.2. Also, the variables that are to be obtained by the inversion are the stiffnesses and not the phase angles or wave normals associated with a desired group-velocity direction. Another difference between the problems is that this inversion is attempting to solve for 21 independent parameters instead of two. Since we are now solving for many more variables, 21 instead of two, there may be some instability in the solution. To stabilize the inversion process, a small scalar quantity λ , is added to the diagonals of the matrix to be inverted in order to dampen the solutions. This damping factor is added into equation 3.4 to give

$$\bar{\Delta} = [\bar{\alpha}^T \bar{\alpha} + \lambda I]^{-1} \bar{\alpha}^T \bar{\delta}g. \quad 3.7$$

Because of all of the numerical calculation of derivatives and the numerical inversion of a large matrix, this operation is computationally fairly cumbersome. What makes this process extremely computer-intensive is the inversion used to calculate the group velocity at a prescribed direction every time a group velocity or a derivative of the group velocity with respect to a stiffness parameter needs to be calculated.

3.2.2 Stiffnesses from phase velocities

The method discussed here for calculating the 21 independent stiffnesses is a least-squares inversion for stiffnesses from group velocities. In the case where phase velocities are measured, like in the experiments done at the Institut Français du Pétrole (Arts, 1993), the same scheme is utilized for the inversion. The exception is that the phase velocities may be calculated directly so the effort and computer time involved in finding a velocity in the appropriate direction is not required.

The calculation of stiffnesses from phase velocities works like the same calculation from group velocities outlined in section 3.2.1. The only change required in the algorithm is the substitution of the phase-velocity magnitude v for the group-velocity magnitude g in equation 3.7. After the appropriate substitutions are made, this equation for the corrections to the stiffnesses becomes

$$\bar{\Delta} = [\tilde{\alpha}^T \tilde{\alpha} + \lambda I]^{-1} \tilde{\alpha}^T \tilde{\delta}v \quad 3.8$$

where

$$\delta v_i = v_i^{obs} - v_i^{calc}, \quad \alpha_{ji} = \frac{\partial v_i}{\partial C_j}, \quad \text{and } \Delta_i = \Delta C_i. \quad 3.9$$

This inversion is 200 to 500 times faster than the same inversion from group velocities due to the absence of the search for a group velocity at each step of the program. Also, these calculations are able to yield a more numerically accurate result because the velocities are calculated directly and exactly instead of being estimated from a least-squares inversion. An additional bonus in this method is that there are no limitations in the calculation of velocities even at or near singularities, where there can be problems when calculating the group velocity in a prescribed direction.

3.2.3 Error analysis

In performing the inversion, it is desirable to know how well the velocities that are calculated from the stiffnesses match the observed velocities, i.e. how well the model fits the data. A statistical velocity error is defined to quantify the goodness of fit. Also, once a set of stiffnesses is determined, a statistical estimate of the uncertainty in each stiffness will need to be calculated.

The velocity error for each iteration is simply defined here as the standard deviation between the measured and calculated velocities σ , which, modified from Kanasewich (1985), is

$$\sigma = \sqrt{\frac{1}{N - (M + 1)} \left(\bar{\delta}g^T \bar{\delta}g - \bar{\Delta}^T \bar{\alpha}^T \bar{\delta}g \right)}, \quad 3.10$$

where N is the number of measurements and M is the number of model parameters that are to be solved for; $M = 21$ in this general case.

Once the standard deviation has been calculated for the experimental observations, the uncertainties for the calculated model parameters, in this case stiffnesses, are calculated from the diagonal elements of the covariance matrix, C_M , which is defined (Jenkins and Watts, 1968; Kanasewich, 1985) as:

$$\tilde{C}_M = [\tilde{\alpha}^T \tilde{\alpha}]^{-1} \sigma^2. \quad 3.11$$

Each diagonal element of the covariance matrix is the variance of the respective inverted stiffness. By assuming a near-Gaussian distribution of error, the square root of each variance is used as an estimate of the uncertainty in the respective stiffness.

3.3 Numerical testing of the algorithm

Numerical forward models generated for materials with known stiffnesses were used to test the algorithm and find its limitations. Tests were performed on both the group- and phase-velocity inversions using velocities calculated from stiffnesses from the orthorhombic industrial laminate used in the experiments of Brown et al. (1993) shown here in table 3.1.

	Forward model stiffnesses (GPa)					
	n=1	n=2	n=3	n=4	n=5	n=6
m=1	17.521	7.220	6.608	0.000	0.000	0.000
m=2	7.220	15.777	6.196	0.000	0.000	0.000
m=3	6.608	6.196	11.750	0.000	0.000	0.000
m=4	0.000	0.000	0.000	3.127	0.000	0.000
m=5	0.000	0.000	0.000	0.000	3.483	0.000
m=6	0.000	0.000	0.000	0.000	0.000	3.804

TABLE 3.1 Stiffnesses used in calculating numerical velocity models for inversion testing.

3.3.1 Phase-velocity inversion

The testing starts with the simplest case, the inversion from phase velocities. The numerical-model phase-velocity data were generated on a grid of azimuths and colatitudes with a 45° grid spacing. For the inversion, the damping factor λ is 10^{-4} GPa and is decreased by 50% for each successive iteration. It took 13 iterations to arrive at a solution accurate to ± 0.001 GPa.

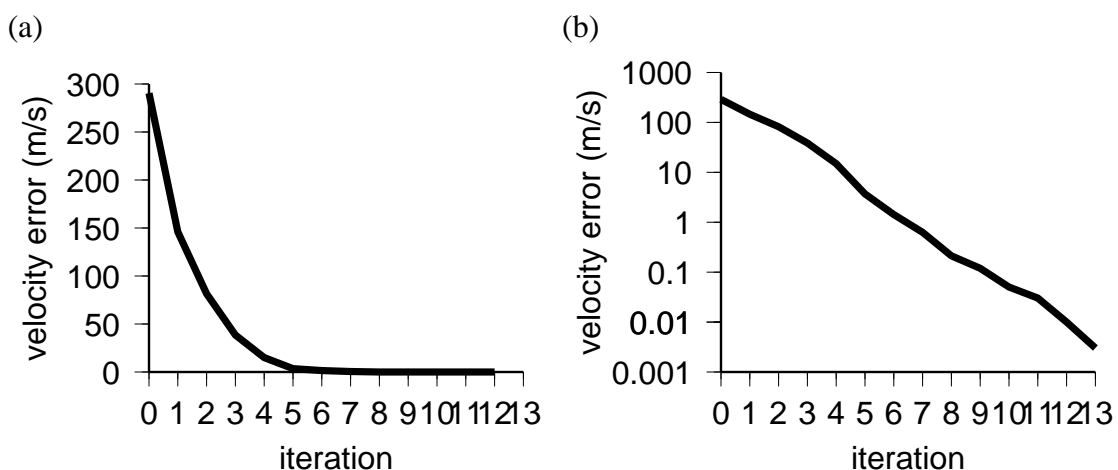


FIG. 3.1 Plots of the velocity error from the phase-velocity inversion. (a) Velocity error versus number of iteration. (b) \log_{10} of the velocity error versus number of iteration.

Figure 3.1 shows graphs (Wessel and Smith 1991) of the velocity error over the course of the inversion process. Figure 3.1b, a logarithmic plot, shows an approximately

straight line with a negative slope which further supports the interpretation that the linear-scaled curve (figure 3.1a) is an exponential-decay curve. Since the error decays exponentially, it takes relatively few iterations to get close to a solution and several more iterations to get a solution with acceptable accuracy. The problem of deciding when to stop iterating and accept the current solution will be more predominant when dealing with laboratory data that contain experimental errors.

(a)	Stiffnesses at the 3rd iteration (GPa)						Error in the stiffnesses (GPa)					
	n=1	n=2	n=3	n=4	n=5	n=6	n=1	n=2	n=3	n=4	n=5	n=6
m=1	16.19	6.42	6.48	0.30	0.05	0.13	0.54	0.52	0.48	0.48	0.42	0.46
m=2	6.42	15.16	6.19	0.19	0.10	-0.08	0.52	0.53	0.45	0.42	0.48	0.47
m=3	6.48	6.19	12.61	-0.22	-0.03	-0.16	0.48	0.45	0.46	0.41	0.39	0.37
m=4	0.30	0.19	-0.22	3.11	0.08	0.06	0.48	0.42	0.41	0.23	0.18	0.26
m=5	0.05	0.10	-0.03	0.08	3.50	-0.02	0.42	0.48	0.39	0.18	0.23	0.27
m=6	0.13	-0.08	-0.16	0.06	-0.02	4.00	0.46	0.47	0.37	0.26	0.27	0.22

(b)	Final inverted stiffnesses (GPa)						Error in the stiffnesses (GPa)					
	n=1	n=2	n=3	n=4	n=5	n=6	n=1	n=2	n=3	n=4	n=5	n=6
m=1	17.521	7.220	6.608	0.000	0.000	0.001	0.0001	0.0001	0.0001	0.0001	0.0001	0.0003
m=2	7.220	15.777	6.196	0.000	0.000	-0.001	0.0001	0.0001	0.0001	0.0001	0.0001	0.0003
m=3	6.608	6.196	11.750	0.000	0.000	0.000	0.0001	0.0001	0.0001	0.0001	0.0001	0.0001
m=4	0.000	0.000	0.000	3.127	0.000	0.000	0.0001	0.0001	0.0001	0.0000	0.0000	0.0000
m=5	0.000	0.000	0.000	0.000	3.483	0.000	0.0001	0.0001	0.0001	0.0000	0.0000	0.0000
m=6	0.001	-0.001	0.000	0.000	0.000	3.804	0.0003	0.0003	0.0001	0.0000	0.0000	0.0000

TABLE 3.2 Stiffnesses (a) after 3 iterations of the phase-velocity inversion and (b) the final inverted stiffnesses with their respective error estimates.

Table 3.2a shows the stiffnesses resulting from the third iteration of the inversion process with an error estimate for each respective stiffness. At this iteration, the velocity error is 81 m/s, 3.5% of the average velocity. The mean stiffnesses error, however, is 15% of the average stiffness. From this example, which shows the sensitivity of the stiffness error to the error in velocities, it is evident that accurate velocity measurements are important if reasonable stiffnesses are to be calculated.

Table 3.2b shows the stiffnesses after 13 iterations where the inversion is assumed to have converged. The stiffnesses are almost exactly the same as the input model stiffnesses (table 3.1).

3.3.2 Group-velocity inversion

The testing of the group-velocity inversion is approached in a similar manner but,

since this algorithm is more complicated than the phase-velocity inversion and the velocity calculation is not exact, the expectations for the performance of this inversion will be different than for the phase-velocity inversion.

The forward-model group velocities were calculated using the same stiffnesses and data grid as were used for the test of the inversion from phase velocities. Again, an attempt is made to minimize the velocity error defined in equation 3.10.

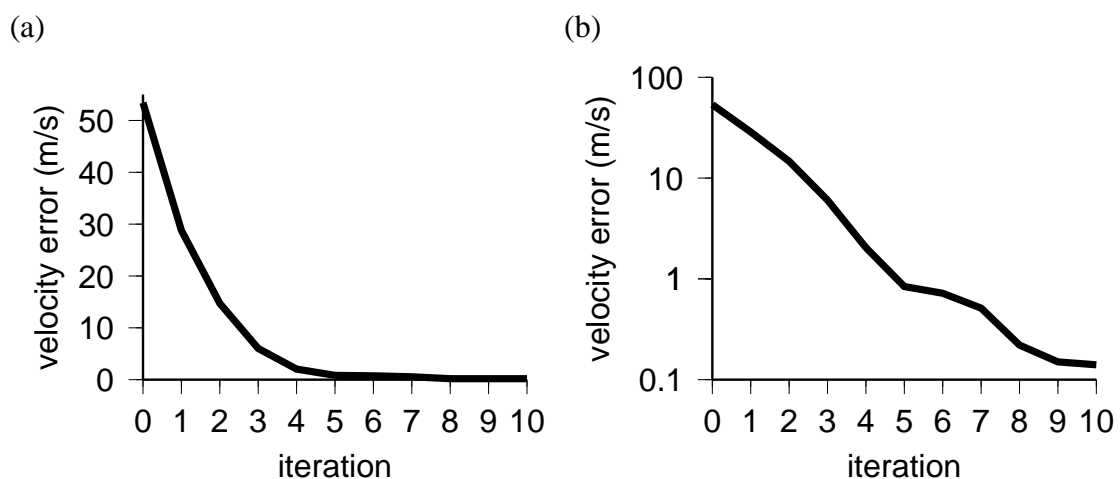


FIG. 3.2 Plots of the velocity error from the group-velocity inversion. (a) Velocity error versus number of iteration. (b) \log_{10} of the velocity error versus number of iteration.

	Final inverted stiffnesses (GPa)						Error in the stiffnesses (GPa)					
	n=1	n=2	n=3	n=4	n=5	n=6	n=1	n=2	n=3	n=4	n=5	n=6
m=1	17.522	7.220	6.609	0.000	0.000	0.000	0.001	0.001	0.001	0.002	0.001	0.001
m=2	7.220	15.777	6.197	0.000	0.001	0.000	0.001	0.001	0.001	0.004	0.003	0.001
m=3	6.609	6.197	11.751	0.000	0.000	0.000	0.001	0.001	0.001	0.002	0.001	0.000
m=4	0.000	0.000	0.000	3.127	0.000	0.000	0.002	0.004	0.002	0.001	0.000	0.002
m=5	0.000	0.001	0.000	0.000	3.484	0.000	0.001	0.003	0.001	0.000	0.001	0.001
m=6	0.000	0.000	0.000	0.000	0.000	3.804	0.001	0.001	0.000	0.002	0.001	0.000

TABLE 3.3 Stiffnesses from the group-velocity inversion and their respective error estimates.

Figure 3.2 shows the convergence of the algorithm to a solution where the velocity error becomes negligible. It took only 10 iterations for the changes in stiffnesses from one iteration to the next to become so small that the program stopped. In figure 3.2b one can see that as the algorithm approached a solution, the drop in error is no longer an

exponential-decay curve as the accuracy limit of this method is reached. The velocity errors after the ninth and tenth iterations are 0.15 and 0.14 m/s, respectively, making an improvement much less than the 40% improvement in error per iteration that most of the earlier iterations yielded. This diminishing improvement per iteration confirms the algorithm's decision to stop iterating and assume that it has converged on a solution.

The inverted stiffnesses from this group-velocity inversion are listed in table 3.3. The resulting stiffnesses are very close to the input model stiffnesses and the differences between the computed and model parameters are well within the range of the estimated error.

3.4 Conclusions

A method has been developed to calculate the twenty-one independent elastic stiffnesses from either group or phase velocities. This method is general in the sense that it requires no prior knowledge of the symmetry class of the medium and no prior knowledge of the polarization of the individual wave phases. The which-came-first criterion is used to decide which velocity is associated with a particular wave phase in the sense that the qP is the first or primary phase, the qS₁ is the secondary phase and the qS₂ is the third phase.

An additional inversion step is necessary for the group-velocity inversion since the group velocity cannot be directly calculated in a prescribed direction. This search for a group velocity adds computational complexity and decreases the accuracy of the inversion. Even though the group-velocity inversion is not as robust or as accurate as the phase-velocity inversion, the inversion of the numerical-model data yielded stiffnesses nearly identical to the input model stiffnesses.

Both inversions converged quickly and yielded very accurate results when applied to numerical-model velocities. Now we can look at how the inversion method performs in the real world of laboratory data.

Chapter 4

Application of the Inversion to Laboratory Measurements

Two experiments were performed to obtain each of phase and group velocities for the two methods of inversion for material properties. Velocity data were acquired in each experiment for all three wave phases, qP , qS_1 , and qS_2 , in Phenolic CE, the industrial laminate described in Chapter 1.

The first experiment, designed for the acquisition of phase velocities, involved the measurement of traveltimes between large transducers on flat parallel faces of a small (9.6 cm) bevelled cube of phenolic. Nine measurements were made on the 18-sided block for each wave phase yielding 27 velocity measurements for input into the inversion.

Group velocities were calculated from the traveltimes of the second experiment which involved smaller transducers transmitting ultrasonic waves through a larger (23-cm diameter) sphere of the industrial laminate. Traveltimes were acquired on the sphere with transducers at antipodes. Measurements were made at 15° spacing along lines of equal azimuth which were spaced 45° apart, so that data were collected in the yz plane, the zx plane and in a plane bisecting the angle between the yz and zx planes. The resulting 105 data points were used for the inversion from group velocity to stiffnesses.

4.1 Phase-velocity measurements

Figure 4.1 shows photographs of the cube with the bevelled edges and the large transducers used in the experiment. The measurements of traveltimes were across the sample between opposite faces which are approximately parallel. The 18 faces of the cube enabled the experimenters to make nine such traveltime measurements for each wave phase, including three in the principal-axis directions and six measurements at angles bisecting each axis pair.

When designing this experiment, large transducers were chosen to try to ensure

that phase traveltimes would be measured across the sample. The shear-wave transducers have a diameter of 3.8 cm and the compressional-wave transducers are 5 cm in diameter. The qP sources and receivers cannot be considered to be this large, however, because the faces on the sample are only 4 cm across. The maximum group-minus-phase angle, δ_m , that allows determination of phase velocity (equation 2.6) is 21.6° for qS waves and 22.6° for qP waves, if phase velocities are to be acquired. It was shown in chapter 2 (table 2.1) that the largest angle between the group- and phase-velocity vectors is 11.6° for this medium which is close to half of δ_m ; so there should be no doubt that the measured traveltimes are phase traveltimes.

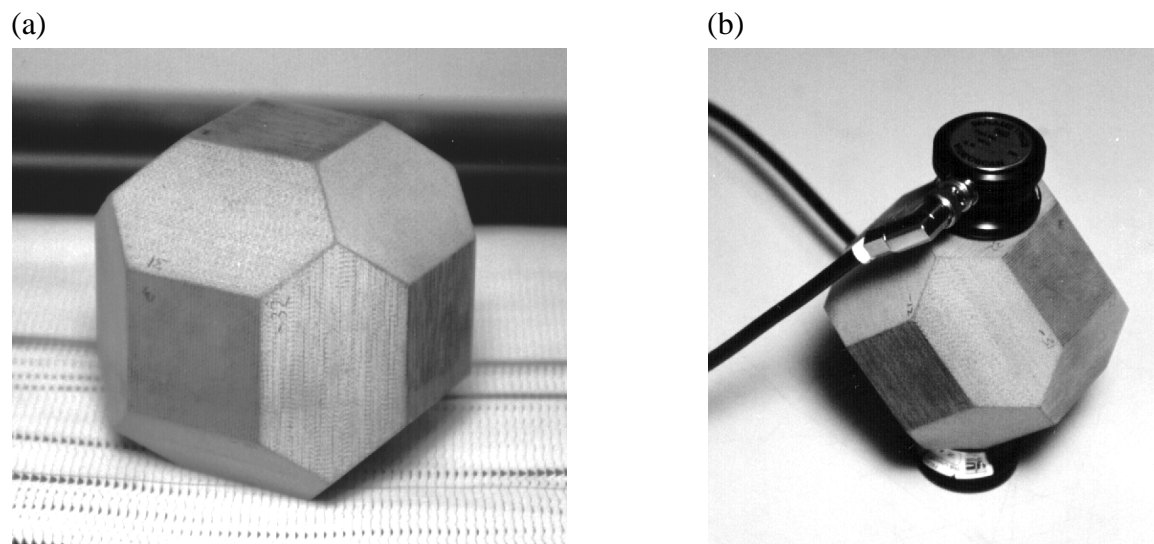


FIG. 4.1 (a) Bevelled cube of Phenolic CE. (b) The large transducers used to obtain phase traveltimes.

Traveltimes were measured as the time elapsed between pulse initiation and the arrival of the first discernible energy in the waveform on the oscilloscope. The time is determined to three significant figures, the first arrivals being picked to the nearest $0.1 \mu\text{s}$, with an uncertainty in the pick of around $\pm 0.5 \mu\text{s}$. The distances have an uncertainty of a few tenths of a millimeter because of the thin layer of coupling agent between the transducers and the cube. The uncertainty in the calculated laboratory velocities based on uncertainties in distance and time measurements is estimated at $\pm 2\%$.

The algorithm was applied to the velocity data and the inversion converged at a velocity error (defined by equation 3.10) of 18.0 m/s , less than 1% of the average velocity which is well within the estimated experimental uncertainty of $\pm 2\%$. The resulting stiffnesses and their statistical uncertainties are listed in table 4.1. If the statistical error

estimates in the stiffnesses appear high, this may be caused by the inversion being only somewhat overdetermined. With 27 measurements to determine 21 parameters, there are only 1.28 times more measurements than the minimum required.

	Final inverted stiffnesses (GPa)						Error in the stiffnesses (GPa)					
	n=1	n=2	n=3	n=4	n=5	n=6	n=1	n=2	n=3	n=4	n=5	n=6
m=1	15.91	6.48	6.10	0.06	-0.08	0.21	0.14	0.13	0.13	0.34	0.14	0.23
m=2	6.48	14.43	5.72	-0.15	-0.05	-0.12	0.13	0.13	0.14	0.18	0.28	0.22
m=3	6.10	5.72	10.88	0.07	0.05	0.15	0.13	0.14	0.12	0.23	0.18	0.26
m=4	0.06	-0.15	0.07	3.05	0.01	0.01	0.34	0.18	0.23	0.05	0.06	0.06
m=5	-0.08	-0.05	0.05	0.01	3.44	-0.02	0.14	0.28	0.18	0.06	0.05	0.08
m=6	0.21	-0.12	0.15	0.01	-0.02	3.76	0.23	0.22	0.26	0.06	0.08	0.05

TABLE 4.1 Stiffnesses estimated by phase-velocity inversion and their associated uncertainties.

Velocities from those stiffnesses and the velocities from the experiment are plotted in figures 4.3a-c for the xy , yz and zx planes, respectively. These graphs show the agreement between the velocities computed from the inverted stiffnesses and the observed velocities.

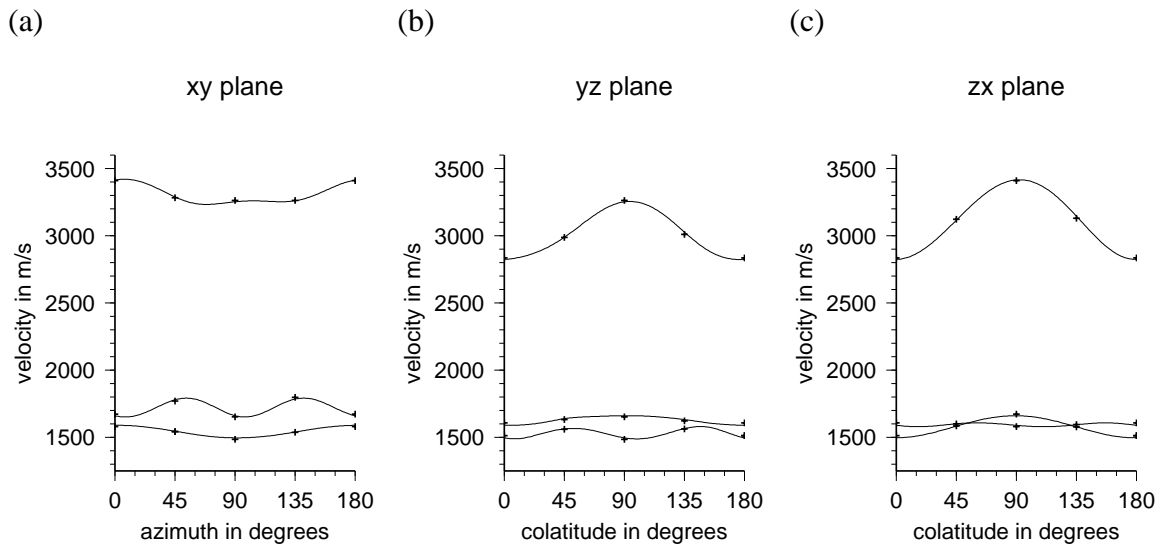


FIG. 4.2 Phase-velocity plots for the phenolic block. The crosses represent the observed velocity data and the solid curves are the phase velocities computed from the inverted stiffnesses.

Collecting the data for this inversion went quickly since only 27 measurements could be made of traveltimes between flat faces with parallel normal vectors without

further carving up the sample. The inversion took a few seconds of computer time making this method of determination of stiffnesses fast and easy. The small velocity error ($< 1\%$), less than the estimated relative experimental error (2%), indicates that this is also an effective method.

4.2 Group-velocity measurements

For the second experiment performed on the phenolic material, a 23-cm diameter sphere of the material was used. This large sphere was manufactured out of two cylinders of the material glued together and machined into a sphere. The glue seam is at the equator of the experimental coordinate system, the xy plane, and holds the top canvas layer of one piece to the bottom canvas layer of the other. It was desirable to make a sphere large enough to gain more clear separation between the two shear arrivals as well as separation between the shear arrivals and the reflected or refracted qP arrivals.

One of the advantages of performing an inversion from group velocities is realized here. Since flat faces and large transducers are not required or even desired in these experiments, a sphere is used and velocity measurements may be taken anywhere on the sphere. This freedom from taking measurements on flat faces has allowed the measurement of traveltimes yielding 105 velocities for the inversion. The sphere was placed in a jig that holds both transducers and has a protractor surrounding the sphere to make it easy to determine where on the sphere the measurements are taken (figure 4.3). Using the protractor, measurements may be taken as closely spaced as every half-degree around the sphere.

After the first arrivals were picked for each wave phase and a few anomalous data points at the glued seam on the equator of the sphere were removed, 99 velocities were used in the final inversion – removing anomalous data is an affordable luxury when one has 105 data points. The velocity error after the final iteration is 7.7 m/s, approximately 0.3% of the average velocity, well within the estimated experimental uncertainty of $\pm 2\%$. The resulting stiffnesses are listed in table 4.2 along with the statistical uncertainties in those stiffnesses which were calculated as described in section 3.2.3. The uncertainties in the stiffnesses for this inversion are substantially lower than the statistical uncertainties calculated from the phase-velocity inversion (table 4.1). This difference in the error in the stiffnesses is probably a result of this inversion being much more overdetermined, with nearly five times as many measurements as number of required parameters.

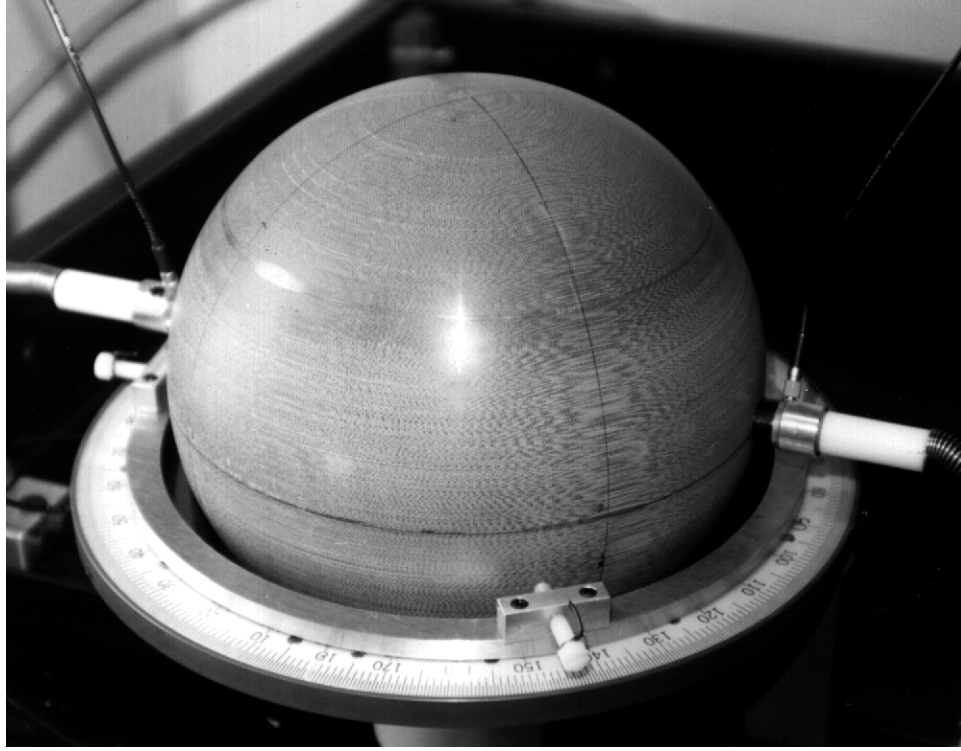


FIG. 4.3 Experimental set-up for measuring group velocities on the sphere. In this jig, the sphere is clamped to a ring inside the protractor and can be rotated about a vertical axis at an increment measured on the protractors.

	Final inverted stiffnesses (GPa)						Error in the stiffnesses (GPa)					
	n=1	n=2	n=3	n=4	n=5	n=6	n=1	n=2	n=3	n=4	n=5	n=6
m=1	16.85	7.88	6.81	0.07	-0.18	0.12	0.06	0.06	0.04	0.05	0.02	0.06
m=2	7.88	16.03	6.51	0.00	-0.26	-0.08	0.06	0.06	0.05	0.02	0.06	0.07
m=3	6.81	6.51	11.14	0.00	-0.05	-0.04	0.04	0.05	0.02	0.01	0.02	0.03
m=4	0.07	0.00	0.00	3.03	0.01	0.04	0.05	0.02	0.01	0.01	0.02	0.02
m=5	-0.18	-0.26	-0.05	0.01	3.40	-0.01	0.02	0.06	0.02	0.02	0.01	0.02
m=6	0.12	-0.08	-0.04	0.04	-0.01	3.89	0.06	0.07	0.03	0.02	0.02	0.02

TABLE 4.2 Final inverted stiffnesses and their respective uncertainties from the group-velocity inversion of the laboratory data.

The data points used for the inversion, as well as the velocity curves from the inverted stiffnesses are graphed in figure 4.4. In these velocity plots the data acquired in the experiment fit rather neatly on the velocity curves calculated from the inverted stiffnesses. The relatively high statistical accuracy of the inversion is likely due to the large number of data points. The consistency of these velocity data is likely also a factor

in the low statistical error result and this is probably a positive side-effect of using a sphere in the experiment. The transducers are moved along the sphere as it is rotated in the jig (figure 4.3) so they stay in contact with the sphere from measurement to measurement with the same couplant between the transducer and the sphere. The experimental set-up is not disturbed as much as it is when removing the transducers from one pair of faces and attaching them to other faces, as done for the phase-velocity measurements.

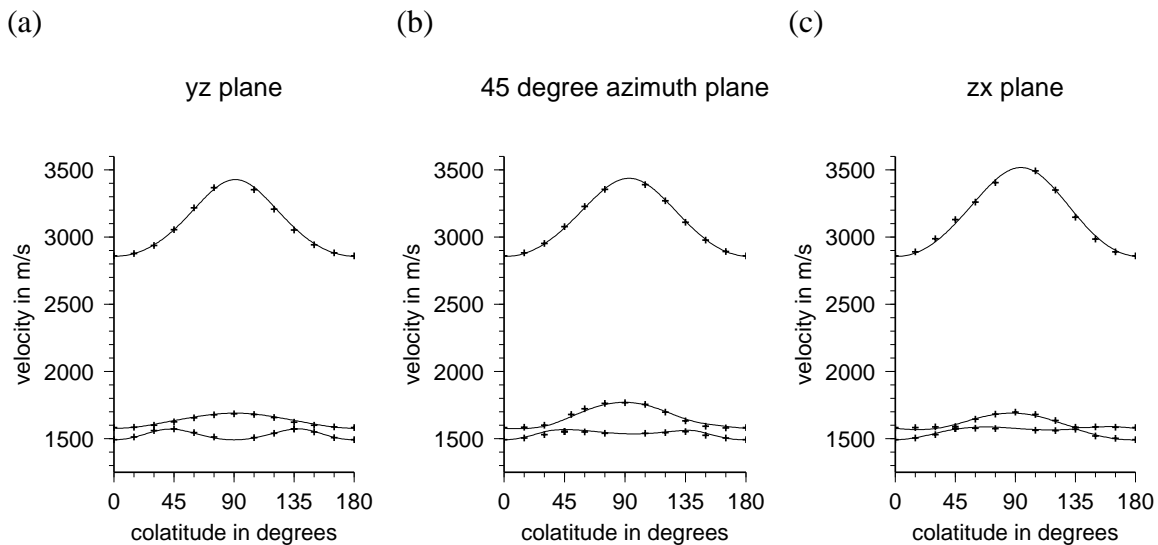


FIG. 4.4 Group-velocity plots for the phenolic sphere. The crosses represent the data points from the experiment and the solid lines are the group velocities from the inverted stiffnesses.

The velocity curves appear to be nearly symmetrical on either side of the equatorial plane or 90° colatitude. The possibility of these symmetries existing is supported by the relatively small values that were calculated for the off-diagonal stiffnesses where m or n is greater than three. If the medium displayed orthorhombic symmetry, these values would be zero and each axis, x , y , and z , would be an axis of symmetry. The likelihood that this medium has orthorhombic symmetry will be discussed in section 4.3.

Despite the lack of robustness and accuracy in the group-velocity-inversion method that was apparent in the numerical example in chapter 3, the inversion yielded relatively accurate stiffnesses with an excellent fit of the model velocities to the velocities measured in the lab. Whatever this inversion lacks in numerical accuracy and stability, it appears to make up for when used on real data. In the measuring of group traveltimes,

there is freedom to take several measurements from many different angles without the need to cut faces into the material whose normals are in the desired direction of wave propagation. It is this freedom to make as many measurements as are desired and the freedom to make the measurements as consistent as possible that redeems this inversion method.

4.3 Why bother with two separate inversions?

It has been shown in chapter 2 (table 2.1) that the difference between group and phase velocities is relatively small ($\approx 2\%$ in that example) even for a medium of moderate ($\approx 20\%$) anisotropy. Arts (1993) performs an experiment where traveltimes are measured through a small (6.5-cm diameter) sphere. He then performs his phase-velocity inversion on the velocities calculated from those traveltimes arguing that there is very little ($< 1\%$) difference between group and phase velocities in a medium with weak ($< 10\%$) anisotropy. The question is: will there be a significant difference a medium of moderate anisotropy between the phase-velocity-inverted stiffnesses and the group-velocity-inverted stiffnesses or is the additional effort involved in the group-velocity inversion a waste of computational time?

In trying to answer this question, an inversion was performed on the velocity data from the large sphere assuming that the velocities are phase velocities. These stiffnesses are then compared with the stiffnesses already derived from the group-velocity inversion. Table 4.3 shows the stiffnesses from the group-velocity inversion (see section 4.2) and the phase-velocity inversion of the same data. The differences between corresponding elements in the stiffness matrix are listed in table 4.4.

	Group-velocity inverted stiffnesses (GPa)						Phase-velocity inverted stiffnesses (GPa)					
	n=1	n=2	n=3	n=4	n=5	n=6	n=1	n=2	n=3	n=4	n=5	n=6
m=1	16.85	7.88	6.81	0.07	-0.18	0.12	16.37	7.47	6.44	0.04	-0.16	-0.01
m=2	7.88	16.03	6.51	0.00	-0.26	-0.08	7.47	15.58	6.20	-0.00	-0.26	-0.11
m=3	6.81	6.51	11.14	0.00	-0.05	-0.04	6.44	6.20	11.03	0.01	-0.03	-0.15
m=4	0.07	0.00	0.00	3.03	0.01	0.04	0.04	-0.00	0.01	3.00	0.04	0.03
m=5	-0.18	-0.26	-0.05	0.01	3.40	-0.01	-0.16	-0.26	-0.03	0.04	3.35	0.01
m=6	0.12	-0.08	-0.04	0.04	-0.01	3.89	-0.01	-0.11	-0.15	0.03	0.01	3.88

TABLE 4.3 Stiffnesses from the group- and phase-velocity inversions of the same data.

	Difference between the stiffnesses (GPa)					
	n=1	n=2	n=3	n=4	n=5	n=6
m=1	0.48	0.41	0.38	0.02	-0.02	0.14
m=2	0.41	0.44	0.31	0.00	0.00	0.03
m=3	0.38	0.31	0.11	-0.00	-0.02	0.11
m=4	0.02	0.00	-0.00	0.03	-0.03	0.01
m=5	-0.02	0.00	-0.02	-0.03	0.04	-0.01
m=6	0.14	0.03	0.11	0.01	-0.01	0.02

TABLE 4.4 Differences between the group-velocity inverted stiffnesses and the phase-velocity inverted stiffnesses.

There appears to be a fairly significant difference in stiffnesses between these two inversions and these differences are not uniform over the entire matrix. For example, the difference between the values for C_{44} , C_{55} , and C_{66} are very small (≤ 0.04 GPa or $\leq 1\%$) compared to the differences between the values for C_{12} and C_{13} which are over 5%.

This exercise shows that there can be a fairly significant difference between the stiffnesses derived from the group-velocity inversion and from the phase-velocity inversion. This difference emphasizes the value of using the correct inversion method with the appropriate type of data. It is theoretically incorrect to perform a phase-velocity inversion on group-velocity data and there can be significant differences between stiffnesses when the wrong type of velocity is assumed in the inversion when dealing with velocities from moderately or highly anisotropic materials.

4.4 Inversion for a not-so-general elastic tensor

The previous work on the phenolic laminate cited here (Brown et al. 1991, 1993; Cheadle et al. 1991) was done assuming that the anisotropy of the material belonged to the orthorhombic symmetry class. In order to investigate whether or not the velocity data obtained in the laboratory may be interpreted as velocities from an orthorhombic medium, an inversion was attempted in which only the nine independent stiffnesses required to define an orthorhombic medium were free to vary.

In the orthorhombic case, the nine independent non-zero stiffnesses in the general

anisotropic stiffness tensor are as follows:

$$C_{mn} = \begin{bmatrix} C_{11} & C_{12} & C_{13} & 0 & 0 & 0 \\ & C_{22} & C_{23} & 0 & 0 & 0 \\ & & C_{33} & 0 & 0 & 0 \\ & & & C_{44} & 0 & 0 \\ & & & & C_{55} & 0 \\ & & & & & C_{66} \end{bmatrix}. \quad 4.1$$

The inversion procedure is identical to that outlined in chapter 3 with the exception that all 12 of the stiffnesses not included in equation 4.1 are held at zero throughout the inversion process. This ensures that the inversion program will derive the best solution for stiffnesses with orthorhombic – or higher order – symmetry.

When the program was run on the group-velocity data from the sphere (section 4.2), the velocity error was minimized at 16.1 m/s. This is more than double the velocity error found in the inversion of the same data for the general elastic tensor, but this is still less than 1% ($\approx 0.6\%$) of the average velocity.

	Final inverted stiffnesses (GPa)						Error in the stiffnesses (GPa)					
	n=1	n=2	n=3	n=4	n=5	n=6	n=1	n=2	n=3	n=4	n=5	n=6
m=1	17.00	7.85	6.65	0	0	0	0.11	0.09	0.06	0	0	0
m=2	7.85	15.97	6.56	0	0	0	0.09	0.10	0.06	0	0	0
m=3	6.65	6.56	11.16	0	0	0	0.06	0.06	0.04	0	0	0
m=4	0	0	0	3.03	0	0	0	0	0	0.02	0	0
m=5	0	0	0	0	3.35	0	0	0	0	0	0.02	0
m=6	0	0	0	0	0	3.88	0	0	0	0	0	0.03

TABLE 4.5 Final inverted stiffnesses and their respective uncertainties from the group-velocity inversion of the laboratory data assuming an orthorhombic medium.

Table 4.5 contains the stiffnesses and uncertainties for the inversion that assumes that the medium is orthorhombic. Note that the stiffnesses are not very different from those calculated in the general inversion (table 4.2), but the uncertainties are almost double the uncertainties associated with the general inversion. This is not surprising, since the velocity error for this inversion is twice that of the previous inversion.

The match of the laboratory velocities to the model velocities does not appear to be quite as good in this case, as seen in figure 4.5, as in the general inversion, shown in figure 4.4. The most significant discrepancy between the model and observed velocities appears to be in the qP-wave velocity. The observed velocities appear to be shifted

slightly to the right in figures 4.4b and 4.4c. This shift of a few degrees in colatitude could be due to an error made while aligning the transducers at the estimated z -axis or zero-colatitude points.

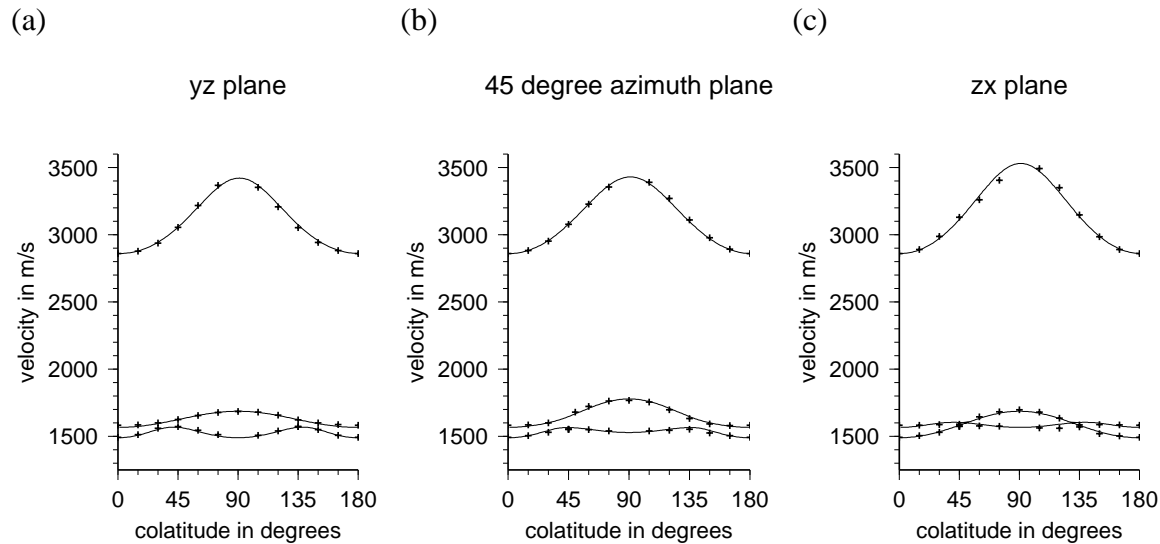


FIG. 4.5 Group-velocity plots for the phenolic sphere. The crosses represent the data points from the experiment and the solid lines are the group velocities from the orthorhombic stiffnesses.

The assumption that this material displays orthorhombic symmetry appears to be quite reasonable. A solution for the stiffnesses of the large sphere was found that fits the data within a reasonable margin of experimental error when orthorhombic symmetry was assumed. The inversion used here is a little faster than the inversion for the general elastic tensor and would be appropriate for media that display cubic, hexagonal or orthorhombic symmetry where the orientation of the principal axes is known.

4.5 Conclusions from the physical-model inversions

Each of the three inversions performed on the data from the two laboratory experiments generated stiffnesses that yield forward-model velocities that match up well with the velocities observed in the laboratory.

Despite the limitations discussed in chapter 3, the group-velocity inversion for the general anisotropic tensor yielded the best results in its inversion of the 99 velocity data-points from the sphere of phenolic. The smallest velocity error (7.7 m/s) and the least

average statistical uncertainty in the stiffnesses (0.04 GPa) came out of this particular application of the algorithm. The excellent performance of this inversion is attributed to the freedom that the experimenter has to make as many measurements in whatever directions as are desirable, without having to cut the sample so that plane waves may be generated.

In contrast to the group-velocity method, the phase-velocity inversion was the most robust and most accurate method in the theory and numerical testing of chapter 3, but did not perform as well when faced with real laboratory data. The only drawback to the application of this method appears to be the limitation of inverting only plane-wave velocities. The model velocities fit the observed velocities with a statistical error of 18 m/s resulting in an average uncertainty in the stiffnesses of 0.16 GPa, statistical errors that are substantially higher than those for the group-velocity inversion. Despite this higher statistical error due to fewer measurements, the errors from the phase-velocity inversion are still well within the uncertainty estimates for the laboratory measurements.

It was shown here that if we assume that the velocities from the sphere are phase velocities so that we can use the faster and more-accurate phase-velocity inversion, the resulting stiffnesses can be significantly different than the stiffnesses resulting from a group-velocity inversion. Even though there isn't much difference between the group and phase velocities of this moderately anisotropic medium, it is important to use the appropriate inversion when dealing with moderately to highly anisotropic media if accurate stiffnesses are to be calculated.

One additional group-velocity inversion was performed on the data from the phenolic sphere to see how well the model would fit the data if the medium were constrained to be orthorhombic, with the symmetry axes coincident with the coordinate axes used in the experiment. This orthorhombic model fits very well to the observed velocity data. The velocity error of 16.1 m/s, 0.6% of the average velocity, is well within the experimental error estimate of $\pm 2\%$. From this inversion exercise one may conclude that the assumption of orthorhombic symmetry appears to be valid for this medium.

Chapter 5

Conclusions

If laboratory measurements of traveltimes are to be performed on anisotropic rocks or physical models to determine stiffnesses, it is very important to know how to interpret the observed traveltimes in terms of group or phase velocities. With consideration of this problem early on in an anisotropic study, one may avoid the complications unforeseen by Cheadle et al. (1991). In that experiment the measurements were assumed to be of group traveltimes between source and receiver centers, but were, in reality, measurements of phase traveltimes in most of the cases and in two cases measurements of group traveltimes from one edge of the source transducer to the other edge of the receiver transducer.

Once my numerical models had shown what was happening to the wavefronts as they travelled through the anisotropic medium, a geometric analysis of this effect established a criterion to decide whether group or phase traveltimes or neither are measured in ultrasonic transmissions in the laboratory. Using this criterion in advance of doing any laboratory work, the experiments may be designed to specifically measure either phase traveltimes or group traveltimes.

This experimental design has been implemented in the laboratory work done for this thesis. One experiment, using large transducers with a small normal separation, was designed to acquire phase velocities while a second experiment, using small transducers on a much larger sample, was designed specifically to acquire group velocities. These velocities were then used to obtain stiffnesses of the material using numerical inversions from each of group and phase velocities.

The numerical group-velocity inversion algorithm was designed to overcome the limitations imposed by the fact that group velocities cannot be calculated in a prescribed direction. Jech (1991) designed a similar method but, because of the difficulty in finding a group velocity near shear-wave singularities, performed his inversion using only qP-wave velocities. By using a random search method when the GLI method of finding a group velocity fails, I avoid the problem of relying on the surface characteristics to direct the algorithm towards a solution. Even though this type of search is computer-intensive,

the GLI method only fails a small percentage of the time, depending on the medium, so it does not make a very significant difference in the computational time of the program.

The phase-velocity inversion was designed in a manner similar to that of the group-velocity inversion, with the exception that the phase velocity may be calculated directly for any prescribed direction. In the numerical testing of the algorithm, the inversion from phase velocities was faster and more accurate than the inversion from group velocities. However, the limitations that are imposed in the collection of phase traveltimes in the laboratory give the group-velocity inversion definite advantages in the application to real data.

The results from the group- and phase-velocity inversions indicate that the freedom to make measurements of group velocities in any direction as desired made the results from the group-velocity inversion more accurate when used on laboratory data. Even though the phase-velocity inversion is more straightforward, more accurate and more numerically stable, the difficulty in collecting plane-wave traveltimes in the laboratory makes this method less attractive than the group-velocity inversion. The phase velocities are more mathematically straightforward to calculate, but group velocities are easier to measure.

Once I completed the design of the group-velocity inversion and tested it on numerical and physical models, it was modified to invert for the nine stiffnesses required to define an orthorhombic medium. The purpose of this exercise was to determine whether imposing the assumption of orthorhombic symmetry on the solution yields as good a solution as the assumption of triclinic symmetry. For the 99 velocities used in the inversion, the coefficient of variation from the inversion was less than 1%. This inversion yielded a very reasonable fit which implies that the nine orthorhombic model parameters are sufficient to define this medium. This further implies that the use of additional parameters, i.e. 21 parameters, would be overparameterizing the model and therefore the nine-parameter inversion assuming orthorhombic symmetry is as good as or better than assuming triclinic symmetry.

From this work, we now have a geometrical criterion for determining which of group or phase traveltimes are measured in the laboratory and a new method has been designed for inverting from group velocities to stiffnesses, which has overcome the difficulty of finding the shear-wave group velocity in a prescribed direction near a singularity. During the development of this algorithm, a phase-velocity inversion was designed in order to compare the two methods of acquiring elastic constants – using

phase velocities and using group velocities. This comparison showed the advantages that are realized when using group velocities in the inversion. It has also been shown that the assumption of orthorhombic symmetry appears to be valid for the anisotropic physical-model material Phenolic CE.

References

- Arts, R.J. (1993) "A study of general anisotropic elasticity in rocks by wave propagation: Theoretical and experimental aspects", Ph.D. thesis, Institut Français du Pétrole.
- Arts, R.J., Rasolofosaon, N.J.P., and Zinszner, B.E. (1991) "Complete inversion of the anisotropic elastic tensor in rocks: Experiment versus theory", 1991 Technical Program, 61st Annual International SEG Meeting, Expanded Abstracts, 1538-1540.
- Beltzer, A. I. (1988) *Acoustics of Solids*, Springer-Verlag, Berlin.
- Brown, R.J., Lawton, D.C. and Cheadle, S.P. (1991) "Scaled physical modelling of anisotropic wave propagation: multioffset profiles over an orthorhombic medium", *Geophysics Journal International* **107**, 693-702.
- Brown, R.J., Crampin, S., Gallant, E.V. and Vestrum, R.W. (1993) "Modelling shear-wave singularities in an orthorhombic medium", *Canadian Journal of Exploration Geophysics* **29**, 276-284.
- Cheadle, S.P., Brown, R.J. and Lawton, D.C. (1991) "Orthorhombic anisotropy: A physical seismic modelling study", *Geophysics* **56**, 1603-1613.
- Crampin, S. (1984) "An introduction to wave propagation in anisotropic media", *Geophysical Journal of the Royal Astronomical Society* **76**, 17-28.
- Dellinger, J. (1991) "Anisotropic seismic wave propagation", Ph.D. thesis, Stanford University.
- Dellinger, J. and Vernik, L. (1992) "Do core-sample measurements record group or phase velocity?", 1992 Technical Program, 62nd Annual International SEG Meeting, Expanded Abstracts, 662-665.
- Hayes, M. (1969) "A simple statical approach to the measurement of the elastic constants in anisotropic media", *Journal of Materials Science* **4**, 10-14.
- Helbig, K. (1994) *Foundations of Anisotropy for Exploration Seismics*, Pergamon.
- Jech, J. (1991) "Computation of elastic parameters of anisotropic medium from traveltimes of quasi-compressional waves", *Physics of the Earth and Planetary Interiors* **66**, 153-159.
- Jenkins, G.M., and Watts, D.G. (1968) *Spectral Analysis and its Applications*, Holden-Day.
- Kanasewich, E.R. (1985) *Time Sequence Analysis in Geophysics*, University of Alberta Press.

- Kendall, J-M., and Thomson, C.J. (1989) "A comment on the form of the geometrical spreading equations, with some numerical examples of seismic ray tracing in inhomogeneous, anisotropic media", *Geophysics Journal International* **99**, 401-413.
- Markam, M. F. (1957) "Measurement of elastic constants by the ultrasonic pulse method", *British Journal Applied Physics*, suppl. 6, 56.
- Musgrave, M. J. P. (1959) "The Propagation of Elastic Waves in Crystals and Other Anisotropic Media", *Reports on Progress in Physics* **22**, 74-96.
- Musgrave, M. J. P. (1970) *Crystal Acoustics*, Holden-Day.
- Neighbours, J.R., and Schacher, G.E. (1967) "Determination of elastic constants from sound-velocity measurements in crystals of general symmetry", *Journal of Applied Physics* **38**, 5366-5375.
- Nye, J.F. (1957, 1985) *Physical Properties of Crystals*, Oxford University Press
- Postma, G.W. (1955) "Wave propagation in a stratified medium", *Geophysics* **20**, 780-806.
- Press, W. H., Flannerty, B.P., Teukolsky, S.A., and Vetterling, W.T. (1988) *Numerical Recipes in C*, Cambridge University Press.
- Shuvalov, L. A. (1981) *Modern Crystallography IV: Physical Properties of Rocks*, Springer.
- Thomsen, L. (1986) "Weak elastic anisotropy", *Geophysics* **51**, 1954-1966.
- Twomey, S. (1977) *Introduction to the Mathematics of Inversion in Remote Sensing and Indirect Measurements*, Elsevier Scientific Publishing Co.
- van Buskirk, W.C., Cowin, S.C. and Carter, R. Jr (1986) "A theory of acoustic measurement of the elastic constants of a general anisotropic solid", *Journal of Materials Science* **21**, 2759-2762.
- Voigt, W. (1910) *Lehrbuch der Kristallphysik*, Teubner.
- Wessel, P., and Smith, W.H.F. (1991) "Free software helps map and display data", *EOS, Transactions of the AGU* **72**, 441.
- Winterstein, D.F. (1990) "Velocity anisotropy terminology for geophysicists", *Geophysics* **55**, 1070-1088.